J. Fluid Mech. (2004), *vol.* 519, *pp.* 201–232. © 2004 Cambridge University Press
DOI: 10.1017/S0022112004001247 Printed in the United Kingdom

Distortion of upstream disturbances in a Hiemenz boundary layer

By ZHONGMIN XIONG AND SANJIVA K. LELE

Department of Mechanical Engineering, Stanford University, Stanford, CA 94305, USA

(Received 4 February 2003 and in revised form 24 February 2004)

A theoretical analysis of the distortion of unsteady three-dimensional disturbances in a Hiemenz boundary layer and its effect on the heat transfer enhancement is presented. It is shown that the disturbance length scale is a critical parameter in determining the amplification ratio of the incoming vorticity. For large disturbance length scales, the amplification ratio increases when the length scale decreases, and a maximum value occurs at a length scale close to five times the boundary-layer thickness. The unsteadiness of the disturbances is found to reduce the vorticity amplification, but the effect is second order when the frequency is low compared to the mean flow strain rate. The impinging disturbances induce large-amplitude vorticity of opposite sign at the wall whose magnitude controls the heat transfer enhancement. As an application of the present analysis, a new scaling correlation is derived for stagnation-point heat transfer in the presence of free-stream turbulence. The theoretical correlation, expressed in terms of turbulence intensity, integral length scale and mean flow Reynolds number, agrees reasonably well with recent experimental data.

1. Introduction

The study of fluid flow and heat transfer at a perturbed two-dimensional forward stagnation point provides an improved understanding of the effects of free-stream turbulence in a wide range of engineering problems. In a modern gas turbine engine, for instance, the gas flow exiting the combustor contains high levels of turbulence which cause significant enhancement of heat transfer to the downstream turbine blades (Goldstein 2001), the effect being most severe in the stagnation-point region near the blade leading edge. Efforts to improve the thermal efficiency and reliability of the blade cooling system hinge critically upon an accurate prediction of heat transfer in the presence of free-stream turbulence. Stagnation-point flow also plays an important role in other industrial applications such as material processing and electronics cooling (Nakayama 1995).

Over the years, a number of experiments have investigated the heat transfer enhancement over its laminar value in stagnation-point flows in the presence of free-stream turbulence (see Kestin 1966; Sadeh & Brauer 1980; Van Fossen, Simoneau & Ching 1995; Ames 1997). The turbulence intensity, length scale and the mean flow Reynolds number were shown to be the most important parameters in determining the turbulent heat transfer rate. Typically, the heat transfer enhancement was found to increase with increased Reynolds number and turbulence intensity, but decrease with increased turbulence length scale. Semi-empirical correlations have been proposed to predict the heat transfer enhancement (see for example Smith & Kuethe 1966; Van Fossen *et al.* 1995; Ames 1997). Numerical simulations have also been performed to

study the detailed interaction between free-stream turbulence and a stagnation-point boundary layer. Spalart (1989) found that out of initial white-noise disturbances in a swept Hiemenz boundary layer, the most unstable disturbance-mode is the one that has the same similarity form as the mean Hiemenz flow, i.e. the streamwise velocity is a linear function of the streamwise coordinate x, and the wall normal velocity is independent of x. The flow structures induced by free-stream turbulence in a stagnation region are found to be qualitatively similar to those induced by upstream organized disturbances (Xiong & Lele 2001). The importance of the disturbance length scale has been shown recently through direct numerical simulation of a turbulent stagnation point flow by Bae, Lele & Sung (2003).

The effect of temporal modulation of free-stream velocity was first studied theoretically by Lighthill (1954) who obtained the Stokes-layer corrections for skin friction and heat transfer for a two-dimensional pulsating mean flow about a cylinder. The steady streaming (second-order alteration to the mean flow owing to the Reynolds stresses) in an oscillatory Hiemenz boundary layer was further examined by Grosch & Salwen (1982) and Merchant & Davis (1989), but the emphasis is on finding similarity solutions and the modification to skin friction. The enhancement of heat transfer in a perturbed Hiemenz boundary layer was also conceived as a consequence of flow instability induced by the incoming disturbances. However, Kestin & Wood (1970) found (later, clarified by Wilson & Gladwell 1978), that the two-dimensional Hiemenz boundary layer is always linearly stable to the incoming three-dimensional disturbances. The nonlinear instability was studied by Lyell & Huerre (1985) who showed that if the level of the external disturbances exceeds a certain threshold value, Hiemenz flow can be destabilized. The linear instability for the more general attachment-line boundary-layer flow has also been investigated by Lin & Malik (1996) and Theofilis *et al.* (2003). Morkovin (1979), in a comprehensive review, argued that the enhancement of heat transfer is more likely to be a forced response to the upstream disturbances rather than a result of internal flow instability. The flow visualizations by Nagib & Hodson (1978) and Böttcher & Wedemeyer (1989) strongly support this argument. This viewpoint was advocated earlier by Sutera (1965) who analysed the amplification effect of the mean flow on the incoming disturbances and linked them to the sensitivity of heat transfer to upstream vortical disturbances. By generalizing the classical rapid distortion theory (RDT) (Batchelor & Proudman 1954), Hunt (1973) analysed the second-order moment of the turbulent velocity field when the free-stream turbulence, of either very large or very small integral scales, impinges onto a circular cylinder, but the heat transfer between the fluid and the cylinder was not considered. Dhanak & Stuart (1995) showed that, in the forward stagnation region of any two-dimensional body, the viscous boundary layer can support a substructure of counter-rotating streamwise eddies when there exists weak cross-stream vorticity in the external flow. Kerr & Dold (1994) obtained a family of strained periodic vortex arrays embedded in an inviscid two-dimensional stagnation-point flow. Andreotti, Douady & Couder (2001) have recently used these vortices as a model to study experimentally the dynamics of interaction between strain and vorticity. Although much progress has occurred in understanding the heat transfer augmentation mechanism, there is, to our knowledge, no analytical solution to the impinging vortical disturbances in a viscous Hiemenz boundary layer. Theoretical analysis on the effects of length scale, intensity and frequency of the impinging disturbance and the associated heat transfer has been lacking. This is partly the reason that the prediction of stagnation-point heat transfer in the presence of free-stream turbulence has largely remained empirical. In this paper, the distortion

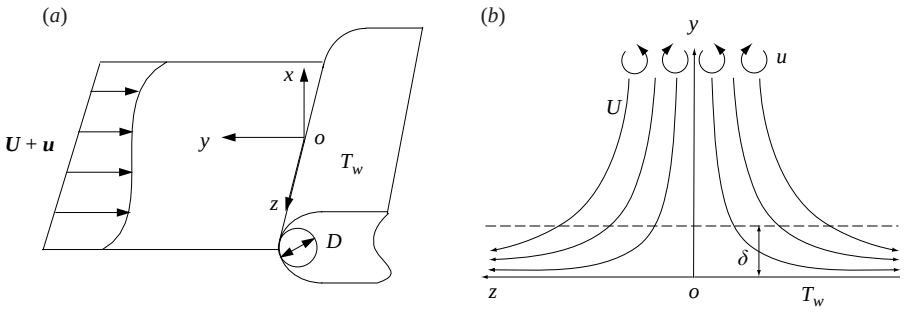

FIGURE 1. (*a*) Disturbed stagnation-point flow at the leading edge of a two-dimensional bluff body. (*b*) Hiemenz boundary-layer flow with upstream incoming disturbances.

of unsteady three-dimensional disturbances in a two-dimensional stagnation- point flow is investigated using theoretical analysis and numerical solutions. Our objective is to gain quantitative understanding of the heat transfer augmentation mechanism, particularly its dependence on disturbance parameters, e.g. length scale, intensity and frequency, as a way to improve the prediction of turbulence effects in this technologically important flow.

The paper is organized as follows. The governing equations for the mean flow and the disturbances are formulated in § 2, followed by a discussion of the length and velocity scales associated with the disturbances. The numerical solutions of the nonlinear disturbance equations, showing the characteristics of the disturbance development, are presented in § 3. Analysis based on linear vortex dynamics is pursued in § 4 to derive the dependence of vorticity amplification on the disturbance length and time scales. In § 5, the asymptotic behaviour for large-scale and low-frequency disturbance is discussed, along with its implications for the wall heat transfer. By superposing different modes of upstream disturbance, the analysis is extended in § 6 to treat the case of homogeneous isotropic free-stream turbulence. A new heat transfer scaling correlation based on the turbulence intensity, integral length scale and Reynolds number is proposed and compared with recent experimental measurements. The conclusions of the present study and a discussion is given in § 7.

2. Governing equations

We consider unsteady incompressible viscous flow with constant fluid properties in the forward stagnation region of an arbitrary two-dimensional bluff body shown in figure 1(*a*). The coordinate axes are chosen as follows: x is parallel to the body and normal to the attachment line, y along the free stream away from the body, and z along the attachment line. The mean flow around the bluff body is assumed to be steady and two-dimensional, but the incoming disturbances are three-dimensional and may vary with time. The length scale of the disturbances is assumed to be large compared with the boundary-layer thickness, but much smaller than the diameter of curvature at the stagnation point, hence the mean flow in this region is modelled well by a plane Hiemenz boundary-layer flow, see for example in Batchelor (1967). Indeed, Wilson & Gladwell (1978) showed that as Reynolds number $Re \to \infty$, the laminar flow in the stagnation region of any two-dimensional bluff body is reduced to a plane Hiemenz flow problem. Exploiting this reduction, the present analysis will be focused on the Hiemenz boundary-layer flow in the presence of upstream disturbances, as shown in figure 1(*b*). By relating the strain rate in the Hiemenz solution to the

free-stream velocity and the diameter of curvature at the stagnation point, the present analysis applies to a general two-dimensional bluff body.

When the characteristic length scale l_0 and velocity scale v_0 of the Hiemenz boundary layer, defined as

$$l_0 = \sqrt{\nu^*/A^*}, \qquad u_0 = \sqrt{\nu^* A^*}, \tag{2.1}$$

are used to non-dimensionalize the coordinates and the flow variables, we have

$$(\xi, \eta, \zeta) = \left(\frac{x^*}{l_0}, \frac{y^*}{l_0}, \frac{z^*}{l_0}\right), \tag{2.2a}$$

$$(\tilde{u}, \tilde{v}, \tilde{w}) = \left(\frac{u^*}{u_0}, \frac{v^*}{u_0}, \frac{w^*}{u_0}\right), \tag{2.2b}$$

$$\tilde{\rho} = \frac{\rho^*}{\rho^*_\infty} = 1, \qquad \tilde{p} = \frac{p^*}{\rho^*_\infty u_0^2}, \tag{2.2c}$$

$$\tilde{\theta} = \frac{T^* - T^*_w}{T^*_\infty - T^*_w}, \tag{2.2d}$$

where the superscript $*$ is used here in after to denote the dimensional quantities, ν^* is the kinematic viscosity and A^* is the strain rate of the external potential flow in the Hiemenz solution. p^* and ρ^* are the pressure and density. The wall is assumed to be isothermal with temperature T^*_w and the upstream flow temperature is T^*_∞.

The flow field $\{\tilde{\boldsymbol{u}}, \tilde{p}, \tilde{\theta}\}$ is assumed to consist of a plane stagnation point flow $\{\boldsymbol{U}, P, \Theta\}$ and a unsteady disturbance field $\{\boldsymbol{u}, p, \theta\}$, i.e.

$$\tilde{\boldsymbol{u}} = \boldsymbol{U} + \boldsymbol{u}, \qquad \tilde{p} = P + p, \qquad \tilde{\theta} = \Theta + \theta, \tag{2.3}$$

Following Batchelor (1967), the mean velocity $\boldsymbol{U}$ of Hiemenz flow may be expressed as

$$\boldsymbol{U} = (U,\ V,\ W) = (\phi'\xi, -\phi, 0). \tag{2.4}$$

Together with the mean temperature Θ, they satisfy the following Hiemenz equations

$$\phi''' + \phi\phi'' + 1 - \phi'^2 = 0, \tag{2.5a}$$

$$\Theta'' + Pr\phi\Theta' = 0, \tag{2.5b}$$

where ϕ is only a function of η and $'$ denotes $\mathrm{d}/\mathrm{d}\eta$. Pr is the Prandtl number. The boundary conditions for ϕ and Θ are given by

$$\phi(0) = \phi'(0) = 0, \quad \phi'(\infty) = 1, \tag{2.6a}$$

$$\Theta(0) = 0, \qquad \Theta(\infty) = 1. \tag{2.6b}$$

The general governing equations for the perturbation field, following from (2.1) and (2.3), can be written as

$$\nabla \cdot \boldsymbol{u} = 0, \tag{2.7a}$$

$$\partial_t \boldsymbol{u} + \boldsymbol{u}\cdot\nabla\boldsymbol{u} + \boldsymbol{U}\cdot\nabla\boldsymbol{u} + \boldsymbol{u}\cdot\nabla\boldsymbol{U} = -\nabla p + \nabla^2\boldsymbol{u}, \tag{2.7b}$$

$$\partial_t\theta + \boldsymbol{u}\cdot\nabla\theta + \boldsymbol{U}\cdot\nabla\theta + \boldsymbol{u}\cdot\nabla\Theta = \frac{1}{Pr}\nabla^2\theta. \tag{2.7c}$$

In this paper, perturbations of the form

$$\boldsymbol{u} = \{u(\eta, \zeta, t)\xi, \quad v(\eta, \zeta, t), \quad w(\eta, \zeta, t)\}, \qquad p = p(\eta, \zeta, t), \qquad \theta = \theta(\eta, \zeta, t), \tag{2.8}$$

are considered; the perturbation variables have no ξ- dependence except for the ξ-component of $\boldsymbol{u}$. As noted by Spalart (1989), this is a good approximation to the flow field in the neighbourhood of the stagnation (η, ζ)-plane. Steady perturbations of this form were also used by Sutera (1965). Substituting (2.8) into (2.7) yields the governing equations for the perturbation field:

$$u + v' + \partial_\zeta w = 0, \tag{2.9a}$$

$$\partial_t u + (u^2 + vu' + w\partial_\zeta u) - \phi u' + v\phi'' + 2u\phi' = u'' + \partial_\zeta^2 u, \tag{2.9b}$$

$$\partial_t v + (vv' + w\partial_\zeta v) - (\phi v)' = -p' + \left(v'' + \partial_\zeta^2 v\right), \tag{2.9c}$$

$$\partial_t w + (vw' + w\partial_\zeta w) - \phi w' = -\partial_\zeta p + \left(w'' + \partial_\zeta^2 w\right), \tag{2.9d}$$

$$\partial_t \theta + (v\theta' + w\partial_\zeta \theta) + v\Theta' - \phi\theta' = \frac{1}{Pr}\left(\theta'' + \partial_\zeta^2 \theta\right). \tag{2.9e}$$

Note here that the prime denotes the partial derivative $\partial/\partial\eta$. The disturbance vorticity may be conveniently found as

$$\omega_\xi = w' - \partial_\zeta v, \qquad \omega_\eta = \xi\partial_\zeta u, \qquad \omega_\zeta = -\xi u'. \tag{2.10}$$

As will be seen in subsequent discussion, the disturbance vorticity in ξ direction ω_ξ, which is subject to stretching by the mean diverging flow, plays a central role in describing the disturbance evolution in this type of flow. Hence, the governing equation for streamwise vorticity, here in after denoted by ω, is written as

$$\partial_t \omega - \left(\omega'' + \partial_\zeta^2 \omega\right) - (\phi\omega)' = -(v\omega)' - \partial_\zeta(w\omega). \tag{2.11}$$

To seek solutions which are periodic in time t (or steady) and periodic in the spanwise direction ζ, we expand u, v, w, ω and θ in a double Fourier series:

$$u(\eta, \zeta, t) = A_p \sum_{m,n=1}^{\infty} u_{mn}(\eta) \exp\{\mathrm{i}(m\sigma_0 t + nk_0\zeta)\} + v_0'(\eta), \tag{2.12a}$$

$$v(\eta, \zeta, t) = A_p \sum_{m,n=1}^{\infty} v_{mn}(\eta) \exp\{\mathrm{i}(m\sigma_0 t + nk_0\zeta)\} - v_0(\eta), \tag{2.12b}$$

$$w(\eta, \zeta, t) = A_p \sum_{m,n=1}^{\infty} (nk_0)^{-1} w_{mn}(\eta) \exp\{\mathrm{i}(m\sigma_0 t + nk_0\zeta)\}, \tag{2.12c}$$

$$\omega(\eta, \zeta, t) = A_p \sum_{m,n=1}^{\infty} \omega_{mn}(\eta) \exp\{\mathrm{i}(m\sigma_0 t + nk_0\zeta)\}, \tag{2.12d}$$

$$\theta(\eta, \zeta, t) = A_p \sum_{m,n=1}^{\infty} \theta_{mn}(\eta) \exp\{\mathrm{i}(m\sigma_0 t + nk_0\zeta)\} + \theta_0(\eta), \tag{2.12e}$$

where A_p is the perturbation amplitude; $k_0 = k^* l_0$ is the fundamental wavenumber in the spanwise direction and $\sigma_0 = \sigma^*/A^*$ is the fundamental frequency. The functions $v_0(\eta)$ and $\theta_0(\eta)$ represent the non-zero spanwise averages of the perturbation velocity and temperature, i.e. the modification to the mean flow profiles owing to the nonlinear interaction among the disturbance modes. Additionally, the normal derivative of $\theta_0(\eta)$ at the wall gives the spanwise- averaged heat transfer enhancement.

Substituting the expansions (2.12*a*) into the continuity equation (2.9*a*) yields

$$u_{mn} + v'_{mn} + \mathrm{i}\, w_{mn} = 0, \tag{2.13}$$

and from the definition of ω_{mn}, it follows that

$$\mathrm{i}\, n^2 k_0^2\, v_{mn} - w'_{mn} + n k_0 \omega_{mn} = 0. \tag{2.14}$$

Similarly, the governing equations for streamwise velocity u_{mn}, vorticity ω_{mn} and temperature θ_{mn} reduce to

$$u''_{mn} - \big(2\phi' + n^2 k_0^2 + \mathrm{i} m \sigma_0\big) u_{mn} + \phi\, u'_{mn} - \phi''\, v_{mn} = \mathscr{N}_0(u, v, w), \tag{2.15}$$

$$\omega''_{mn} - \big(n^2 k_0^2 + \mathrm{i} m \sigma_0\big)\omega_{mn} + (\phi \omega_{mn})' = \mathscr{N}_1(v, w, \omega), \tag{2.16}$$

$$\theta''_{mn} - \big(n^2 k_0^2 + \mathrm{i} m Pr \sigma_0\big)\theta_{mn} + Pr \phi \theta'_{mn} - Pr\, v_{mn} \Theta' = \mathscr{N}_2(v, w, \theta). \tag{2.17}$$

The equations for $v_0(\eta)$ and $\theta_0(\eta)$ can also be derived as

$$v_0''' + \phi v_0'' - 2\phi' v_0' + \phi'' v_0 = \mathscr{N}_3(u, v), \tag{2.18}$$

$$\theta_0'' + Pr \phi \theta_0' = \mathscr{N}_4(v, w, \theta). \tag{2.19}$$

In the above equations, $\mathscr{N}_i$ are the nonlinear terms given by the following expression:

$$\mathscr{N}_0 = \tfrac{1}{2} A_p \sum_{p,q=1}^{\infty} \Big\{ u_{pq} u_{m-p,n-q} + \hat{u}_{pq} u_{m+p,n+q} + v_{pq} u'_{m-p,n-q} + \hat{v}_{pq} u'_{m+p,n+q} + \frac{\mathrm{i}}{q}\big[(n-q) w_{pq} u_{m-p,n-q} + (n+q)\hat{w}_{pq} u_{m+p,n+q}\big] \Big\}, \tag{2.20a}$$

$$\mathscr{N}_1 = \tfrac{1}{2} A_p \sum_{p,q=1}^{\infty} \Big\{ \big[v_{pq}\omega_{m-p,n-q} + \hat{v}_{pq}\omega_{m+p,n+q}\big]' + \frac{\mathrm{i} n}{q}\big[w_{pq}\omega_{m-p,n-q} + \hat{w}_{pq}\omega_{m+p,n+q}\big] \Big\}, \tag{2.20b}$$

$$\mathscr{N}_2 = \tfrac{1}{2} A_p Pr \sum_{p,q=1}^{\infty} \Big\{ v_{pq}\theta'_{m-p,n-q} + \hat{v}_{pq}\theta'_{m+p,n+q} + \frac{\mathrm{i}}{q}\big[(n-q) w_{pq}\theta_{m-p,n-q} + (n+q)\hat{w}_{pq}\theta_{m+p,n+q}\big] \Big\}, \tag{2.20c}$$

$$\mathscr{N}_3 = A_p^2 \sum_{p,q=1}^{\infty} \big[|u_{pq}|^2 + \tfrac{1}{2}(v_{pq}\hat{u}_{pq})'\big], \tag{2.20d}$$

$$\mathscr{N}_4 = \tfrac{1}{2} A_p^2 Pr \sum_{p,q=1}^{\infty} \mathrm{Re}\{\hat{v}_{pq}\theta'_{pq} + \mathrm{i}\hat{w}_{pq}\theta_{pq}\}, \tag{2.20e}$$

where $\hat{}$ stands for the complex conjugate. Suppose that unsteady disturbance vorticity is introduced upstream at $\eta = H_0 \gg 1$ by superimposing a simple sinusoidal variation with the amplitude A_p, at the fundamental spanwise wavenumber k_0, and frequency σ_0 on the mean velocity $\phi(\eta)$. The disturbance boundary conditions at $\eta = H_0$ are

$$v_{11} = 1, \quad v_{mn} = 0 \quad \text{for} \quad m,\, n \neq 1, \qquad u_{mn} = w_{mn} = \theta_{mn} = 0. \tag{2.21}$$

At the wall $\eta = 0$, no-slip and isothermal boundary conditions are enforced for the velocities and temperature, thus

$$u_{mn} = v_{mn} = w_{mn} = \theta_{mn} = 0. \tag{2.22}$$

Once the disturbance velocity v_{mn}, w_{mn} and temperature θ_{mn} are obtained, the relative heat transfer enhancement Δh over its undisturbed mean value h can be found by solving (2.19)

$$\frac{\Delta h}{h} = \frac{\theta_0'(0)}{\Theta'(0)} = -\int_0^\infty \exp\left(-Pr\int_o^\eta \phi\,\mathrm{d}\eta'\right)\int_0^\eta \mathscr{N}_4 \exp\left(Pr\int_o^{\eta'} \phi\,\mathrm{d}\eta''\right)\mathrm{d}\eta'\mathrm{d}\eta. \quad (2.23)$$

It is convenient to introduce new length and velocity scales besides those in (2.1). By the assumed spanwise periodicity, natural choice for-the disturbance length and velocity scales are

$$l_d = 1/k^*, \qquad u_d = \nu k^*. \quad (2.24)$$

It is observed below that the square of the ratio between the disturbance length scale l_d and the Hiemenz boundary-layer scale l_0, represented by a dimensionless parameter λ see Kerr & Dold (1994),

$$\lambda = \left(\frac{l_d}{l_0}\right)^2 = \frac{A^*}{\nu^* k^{*2}} = \frac{1}{k_0^2}, \quad (2.25)$$

is a critical parameter in determining the evolution of the disturbances. When λ is large, the distortion of the upstream disturbances is mainly due to the mean flow straining effect; the nonlinear interaction among the disturbance modes is of higher order. This is similar to the cases treated by the traditional linear RDT; but, in the presence of viscosity, the non-slip wall introduces the viscous effect in its vicinity and must be included in the formulation both for the mean flow and the disturbances. Interestingly, λ can also be interpreted as the time-scale ratio between the disturbance turn-over time l_d/u_d and the mean flow straining time $1/A^*$, i.e.

$$\lambda = \left(\frac{l_d}{u_d}\right)A^*. \quad (2.26)$$

For different values of λ as well as A_p, the numerical solutions to the flow problem posed here are presented in the next section.

3. Numerical results

The system of equations (2.13)–(2.19), with boundary conditions (2.21)–(2.22), forms a second-order boundary-value problem driven by an inhomogeneous boundary condition away from the wall. Numerically, they can be readily solved using the over-relaxation method, described for example in Isaacson & Keller (1993). A fourth-order finite-difference scheme is adopted to approximate the spatial derivatives, and different numbers of grid points ($N = 200, 400$) are used to obtain the grid independent solutions. For the nonlinear calculations, a total number of modes resulting from a truncation at $m = 6, n = 6$ of the double Fourier series in (2.12) are found sufficient for the solutions to converge. The details of the numerical method and convergence study can be found in Xiong (2004).

3.1. *Effects of* λ

The case of steady disturbance, i.e. $\sigma_0 = 0$, is discussed first; this will help clarify the dependence of the disturbance evolution on the length-scale ratio λ. In all

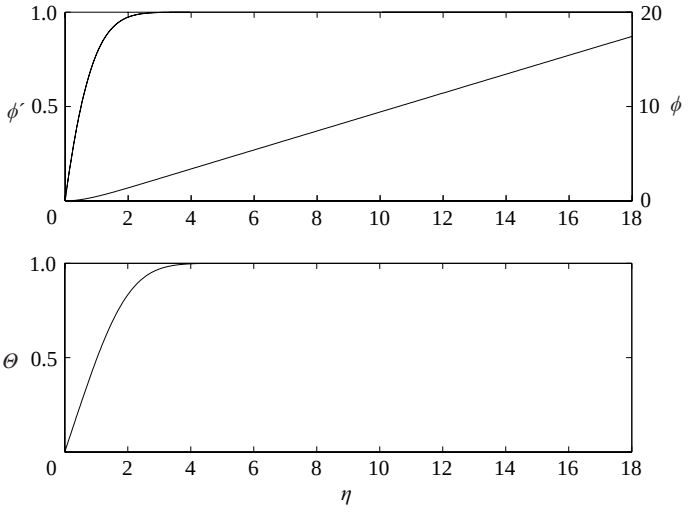

FIGURE 2. Profiles for the mean velocity ϕ, its derivative ϕ' and the mean temperature Θ.

computations, the Prandtl number is taken as $Pr = 0.71$, and the disturbance amplitude Ap is 10% of the mean flow velocity ϕ at the inflow boundary $\eta = H_0$, i.e. $A_p = 0.1\phi(H_0)$ and $H_0 = 18$. Figure 2 shows the profiles of the base state velocity and temperature (without any free-stream disturbance). The velocity and temperature boundary-layer thicknesses (defined as the location at which 99% of the external value is reached) are around $\eta = 2.4$ and $\eta = 4$, respectively. Figure 3 shows the streamline patterns of the perturbed flow in the stagnation plane for different values of λ. The horizontal axis spans one spanwise wavelength for each case.

As can be seen, initially at $\lambda = 1.1$, the perturbed streamlines converge toward a free stagnation point at the symmetry plane $z = 0$. At $\lambda \sim O(2)$, a pair of counter-rotating vortices start to form at the edge of the boundary layer. The strength of these vortices increases rapidly with the increasing λ and attains its maximum at $\lambda = 4$. When λ increases further, the vortex strength slowly decreases. At $\lambda = 32$, the vortices disappear and are replaced again by a sink type free stagnation point. When $\lambda = 64$, the mean flow dominates, and the free stagnation point also disappears. Qualitatively, these streamline patterns can be classified first into two groups depending on whether a free stagnation point (FSP) is present. The stagnation point emerges when the disturbance wall normal velocity v exceeds the mean flow ϕ. Since at the wall, $\phi = \phi' = v = v' = 0$, this can occur when $|v''(0)| \geqslant |\phi''(0)|$. Furthermore, depending on the direction of the spanwise velocity in the neighbourhood of FSP, the resulting FSP can be either a sink point when the spanwise velocity w points inward, or a saddle point when it points outward. Since by symmetry $w \equiv 0$ at $z = 0$, the direction of w is determined by $\partial w/\partial z$. From the continuity equation, this is in turn determined by $\partial v/\partial y$, the rate at which the vertical velocity tends to zero at the free stagnation point. When $\partial v/\partial y < 0$, it becomes a saddle point and the streamlines emanating from the stagnation point eventually form the spiral vortices. For the present case with fixed A_p, the free stagnation point emerges for $\lambda > 1$, and transition from a sink-point to a saddle-point type occurs at $\lambda = 1.6$. At $\lambda = 30$, the saddle-type stagnation point changes back to a sink-point type, causing the vortices to disappear. At $\lambda \geqslant 60$, the free stagnation point also disappears, and the perturbed flow becomes unidirectional in the wall normal direction.

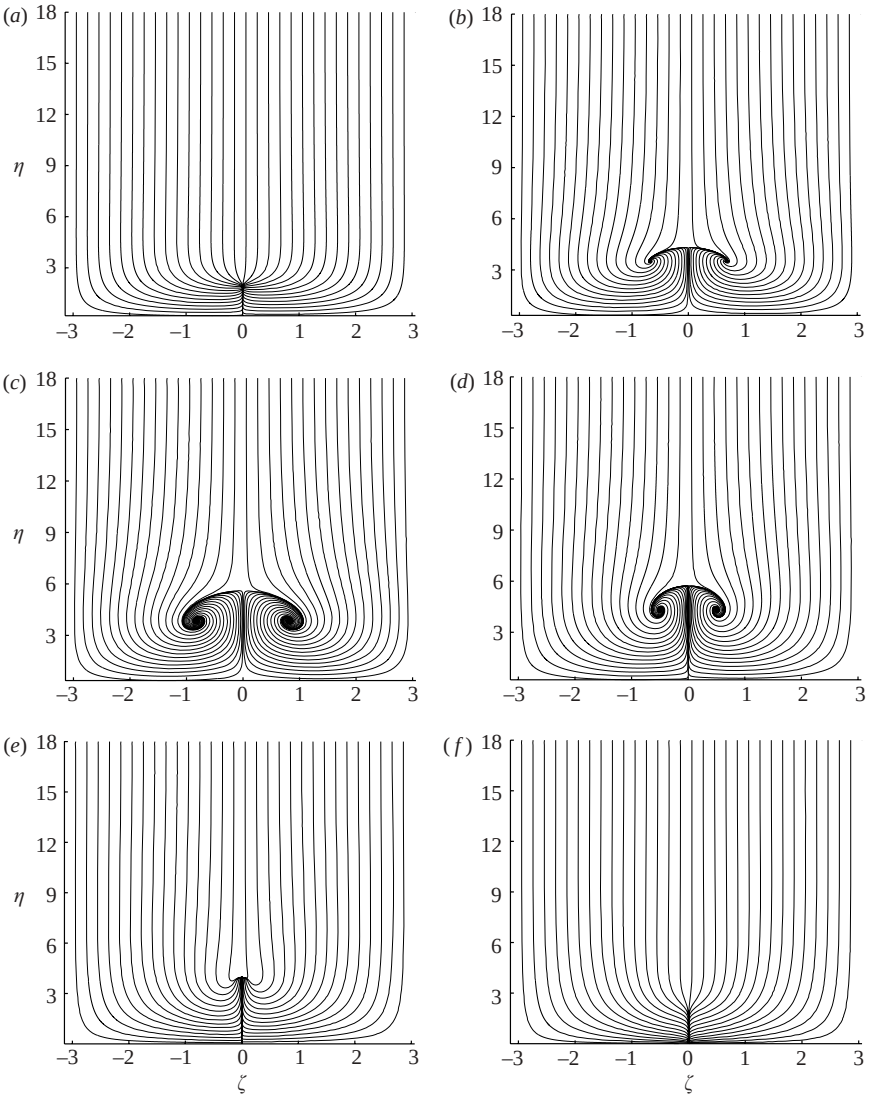

FIGURE 3. Streamline patterns in the stagnation plane for different values of λ. Flow is downward and the spanwise width is one disturbance wavelength. $\lambda = 1.1, 2, 4, 16, 32, 64$ from (a) to (f).

3.2. *Effects of* A_p

In addition to the change of λ, the effect of the disturbance amplitude A_p on the vortex formation is shown in figure 4 where A_p varies from 2% to 15% of $\phi(H_0)$ for fixed $\lambda = 4$. In this case, the free stagnation point first emerges at $A_p = 0.03\phi(H_0)$, and the transition from the sink type to the saddle type takes place at $A_p = 0.05\phi(H_0)$. The latter can be considered as a threshold for A_p since only beyond this value do the counter-rotating vortices become possible in the streamline pattern. Moreover, figure 4 also reveals that although the strength of the vortices increases with increasing A_p, the overall flow pattern remains qualitatively similar once the threshold is reached. The existence of a threshold in disturbance amplitude is also consistent with earlier

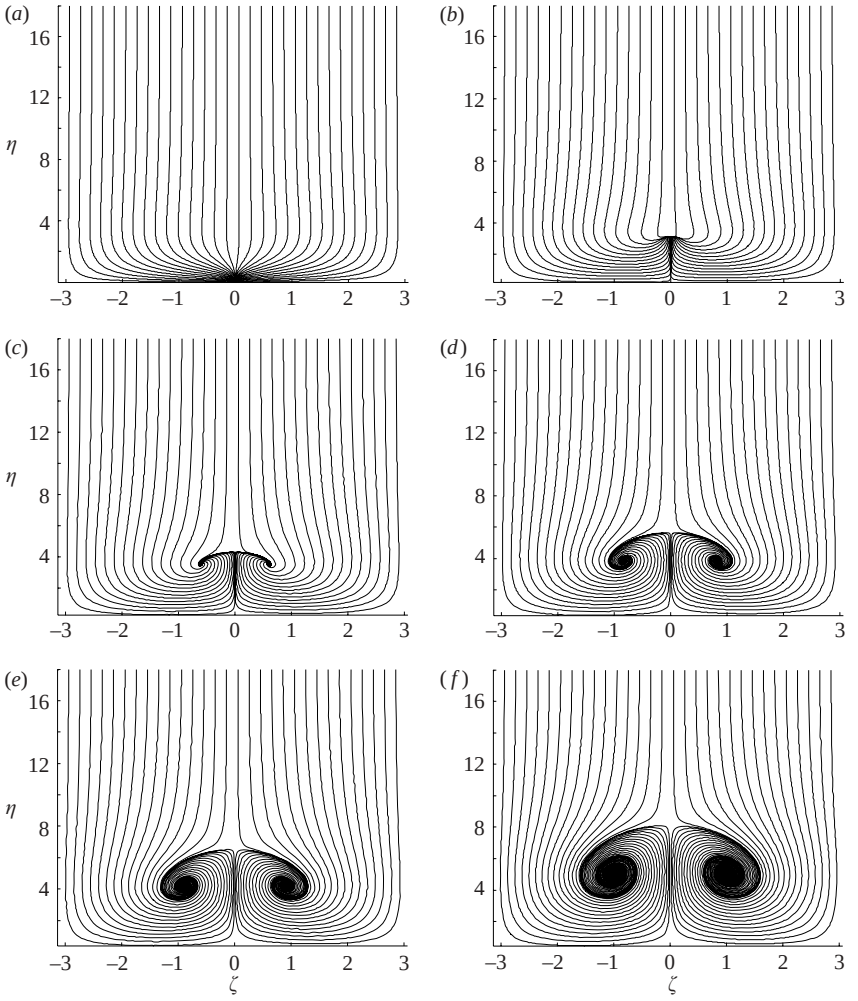

FIGURE 4. Streamline patterns in the stagnation plane for different values of A_p at $\lambda = 4$. Flow is downward and the spanwise width is one disturbance wavelength. $Ap = 0.02, 0.05, 0.07, 0.10, 0.12, 0.15$ from (a) to (f).

observations by Nagib & Hodson (1978) on the formation of a vortex pair at the stagnation region of a bluff body subject to the impingement of wakes. Similar flow patterns as those shown in figures 3 and 4 also emerge in the aforementioned experiments (Nagib & Hodson 1978; Böttcher, J. & Wedemeyer, E. 1989) as well as numerical simulations (Xiong & Lele 2001; Bae *et al.* 2003). The quantitative characterization of the flow fields in figure 4 in terms of the maximum wall normal disturbance velocity $|v_{max}|$, wall vorticity $|\omega_w|$ and heat transfer enhancement $\Delta h/h$ are summarized in table 1.

3.3. *Harmonics and heat transfer*

Figure 5 shows the profiles of the fundamental mode and higher harmonics at $\lambda = 4$ for the disturbance velocity, vorticity and temperature. The disturbance v velocity and vorticity are found to be amplified before reaching the boundary layer. Compared to the fundamental mode $m = 1, n = 1$, the amplitudes of the higher harmonics are

Amplitude $A_p/\phi(H_0)$	Velocity $\lvert v_{max}\rvert$	Vorticity $\lvert\omega_w\rvert$	Heat transfer $\Delta h\,/\,h$
0.02	0.9321	1.4953	0.0100
0.05	2.5558	3.7457	0.0620
0.07	3.8928	5.2490	0.1206
0.10	6.4999	7.5256	0.2406
0.12	8.8094	9.0672	0.3368
0.15	13.729	11.410	0.4918

TABLE 1. The maximum wall normal disturbance velocity $|v_{max}|$, vorticity at the wall $|\omega_w|$ and the heat transfer enhancement $\Delta h/h$ for different A_p at $\lambda = 4$, $H_0 = 18$.

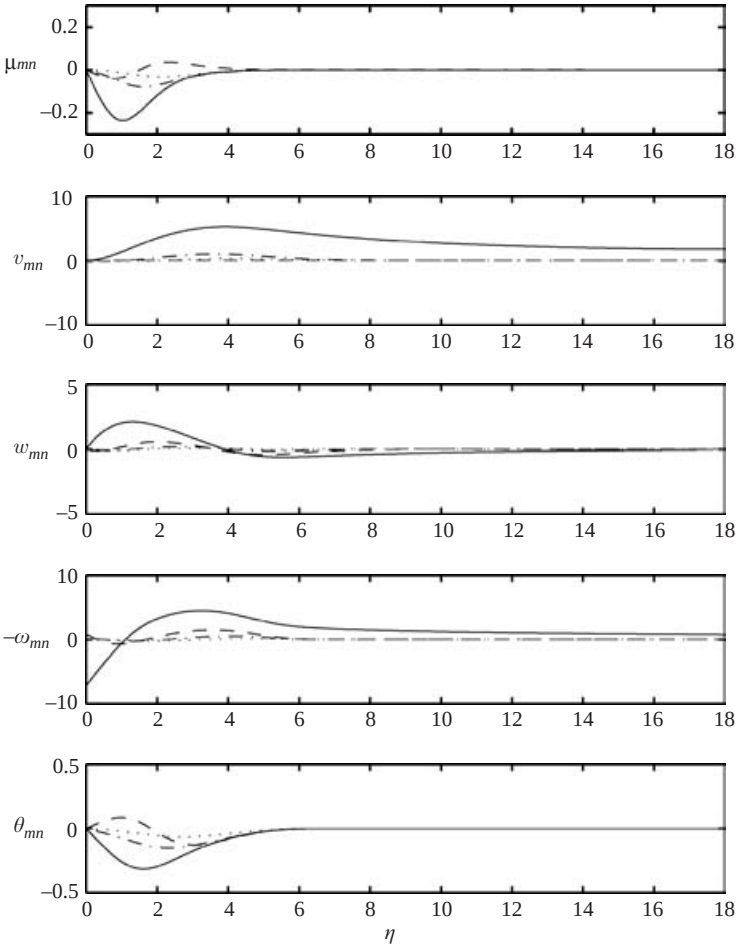

FIGURE 5. Profiles for steady ($\sigma = 0$) velocity and temperature disturbances at $\lambda = 4$. Solid line is the fundamentalmode. The dashed, dash–dot and dotted line correspond to mean flow modification, second and third harmonics for u_{mn}, v_{mn}, θ_{mn}, and second, third and fourth harmonics for ω_{mn} and w_{mn}.

typically small, except for temperature where the mean temperature modification θ_0 attains an amplitude similar to θ_{11}. Of the three components of the disturbance velocity, u_{mn} is found to be typically one order of magnitude smaller than v_{mn} and w_{mn}.

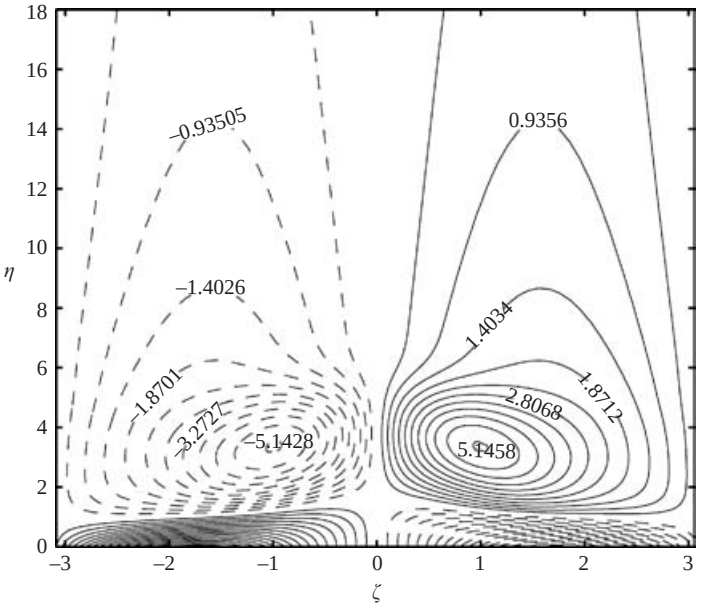

FIGURE 6. Vorticity contours in stagnation plane at $\lambda = 4$, Flow is downward and the spanwise width is 2π. Solid lines are for the positive values of ω and dash lines for the negative.

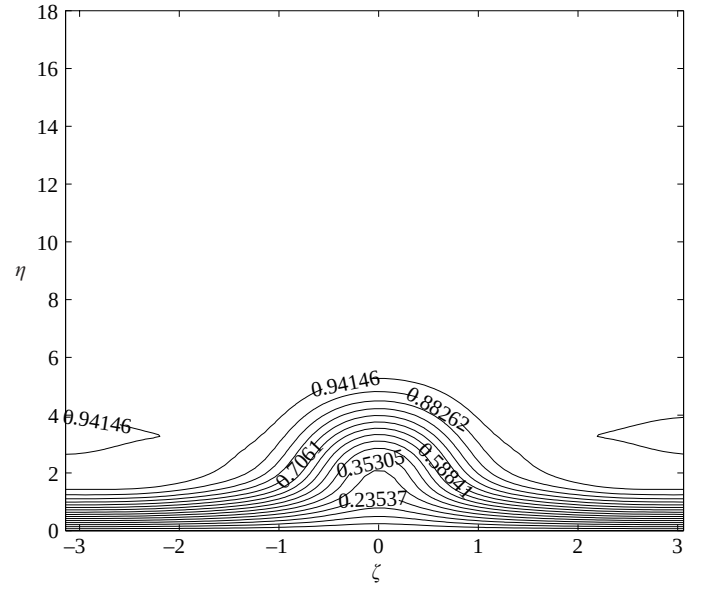

FIGURE 7. Temperature contours in stagnation plane at $\lambda = 4$. Flow is downward and the spanwise width is 2π.

The corresponding contours for the vorticity and temperature are plotted in figures 6 and 7. The incoming vorticity is amplified by a factor greater than 5 owing to stretching and thus large-amplitude vorticity with opposite sign is induced within a thin near-wall region to satisfy the no-slip boundary condition. The temperature contours are

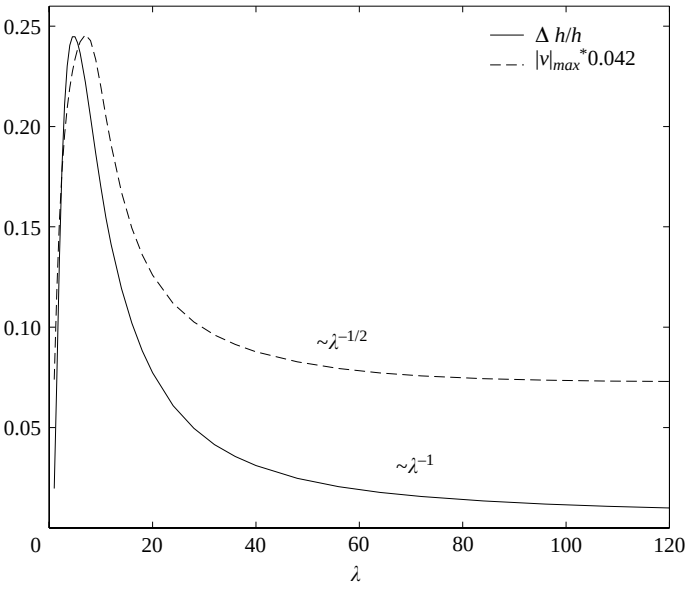

FIGURE 8. Relative heat transfer enhancement $\Delta h/h$ and the maximum amplitude of the fundamental v velocity (renormalized) as a function of λ.

also significantly modified by the disturbance velocity. The upward velocity causes the local thermal boundary layer to become thicker, while the downward velocity makes it thinner. The net effect on the spanwise averaged heat transfer depends on the strength and distribution of these thickened and thinned regions.

In figure 8, the relative heat transfer enhancement $\Delta h/h$ is plotted as a function of λ. For small λ, or small disturbance wavelength, $\Delta h/h$ increases rapidly as λ increases. However, for large λ, it decrease slowly with the increase of λ. A peak value is found around $\lambda = 4$, indicating that an optimum disturbance length scale exists at about five times the boundary-layer thickness and produces maximum heat transfer enhancement. Also shown in figure 8, is the maximum value of the fundamental mode of the disturbance wall normal velocity v_{11}. It shows a similar trend with λ and optimum amplification at nearly the same value of λ. However, for large λ, $v_{max} \sim \lambda^{-1/2}$ while $\Delta h/h \sim \lambda^{-1}$. Finally, in figure 9, the amplitude of the vorticity at the wall is plotted as a function of λ. Besides a similar peak location around $\lambda = 4$, the striking feature of the wall vorticity is that it approaches a constant which depends only on H_0 and A_p as λ becomes large.

The dependence of flow characteristics on the length scale is due to the competition between the vortex stretching and the viscous dissipation. The convective heat transfer or more generally passive scalar transport is a direct consequence of the amplified velocity disturbances, and may in fact be regarded as an indication of how significantly the flow near the wall has been modified. Based on this point of view, the vorticity equation (2.16), comprising the mean flow stretching, viscous dissipation and nonlinear interaction effects, will be the starting point for analysing the disturbance evolution. From the profiles of ω_{mn} in figure 5, the nonlinear interaction is shown to be relatively weak, hence, in the subsequent analysis, the nonlinear terms in (2.16) will be neglected. A similar rationale is also the basis for the linear RDT which has been successfully applied to this type of flow. However, unlike the purely inviscid interaction considered in RDT, in the present problem, viscosity exerts a significant

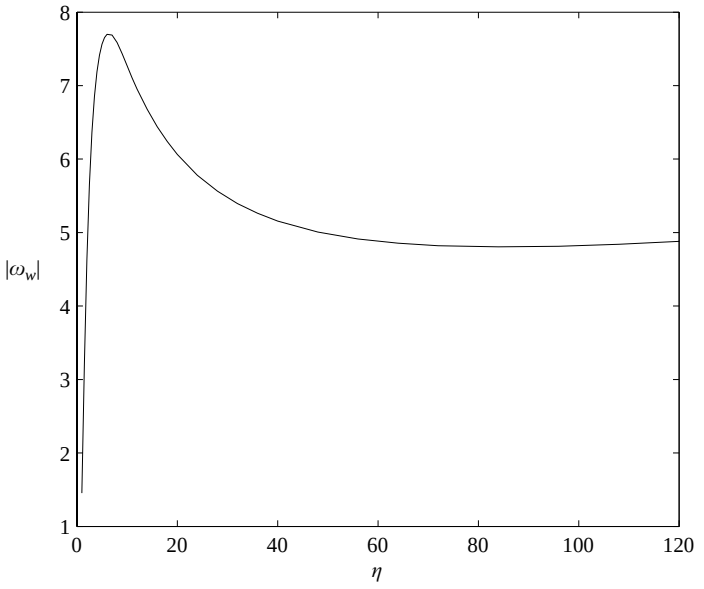

FIGURE 9. Vorticity magnitude at the wall as a function of λ for the steady fundamental mode.

influence upon the disturbance throughout the whole domain, even when the mean flow can be treated largely as inviscid in the region outside the boundary layer. Indeed, it is the balance between the vortex stretching and viscous diffusion that produces the maximum vorticity near the edge of the boundary layer. Therefore, analysis of the vorticity dynamics helps to understand the basic mechanism governing the flow and the associated scalar transport. This is carried out in detail in the subsequent sections.

4. Linear vortex dynamics

The primary goal of the analysis in this section is to find an asymptotic expression describing the evolution of the large-scale low-frequency disturbances in the Hiemenz boundary layer. The solution is sought by first expressing the vorticity in a series expansion based on the large length scale ($\lambda \gg 1$) and low frequency($\sigma_0 \ll 1$). This solution is formally valid in the entire spatial domain, but insufficient to describe the vorticity evolution in an explicit way owing to the lack of a closed-form expression for ϕ. On the other hand, by exploiting the particularly simple form taken by ϕ in the region outside the Hiemenz boundary layer, a closed-form solution for the vorticity can be found for any arbitrary λ and σ_0 in that region. These two solutions are required to match in the region outside the Hiemenz boundary layer where they are both valid. Thus, an explicit composite asymptotic solution can be formulated which describes the evolution of the large-scale low-frequency vortical disturbances, and forms the basis of further analysis.

4.1. *Series expansion*

As shown by the numerical results in figure 5, the disturbance typically reaches its maximum amplitude at the edge of the boundary layer before it decays. By (2.16)

and (2.25), the linearized governing equation for ω_{mn} takes the form

$$\omega''_{mn} - \left(\frac{n^2}{\lambda} + \mathrm{i}\, m\sigma_0\right)\omega_{mn} + (\phi\omega_{mn})' = 0. \tag{4.1}$$

Here only the case of large $\lambda \gg 1$ and small $\sigma_0 \ll 1$ will be considered. These limits correspond to the situation where the upstream disturbance is of large scale and low frequency relative to the Hiemenz boundary-layer scales. This regime is prototypical for the free-stream turbulence impinging on gas turbine blades. A small parameter ϵ may be defined as:

$$\epsilon = \frac{n^2}{\lambda} + \mathrm{i}\, m\sigma_0, \quad |\epsilon| \ll 1, \tag{4.2}$$

and a series solution of ω_{mn} is sought in the powers of ϵ as a regular perturbation:

$$\omega_{mn} = \omega^0_{mn} + \epsilon\omega^1_{mn} + \cdots. \tag{4.3}$$

The equation at zeroth order becomes

$$\left(\omega^0_{mn}\right)'' + \left(\phi\omega^0_{mn}\right)' = 0, \tag{4.4}$$

whose general solution can be found as

$$\omega^0_{mn}(\eta) = E^0\,\mathrm{e}^{-\Phi} + F^0\,\mathrm{e}^{-\Phi}\int_0^\eta \mathrm{e}^{\Phi(\eta')}\,\mathrm{d}\eta'. \tag{4.5}$$

At first order, the equation is

$$\left(\omega^1_{mn}\right)'' + \left(\phi\omega^1_{mn}\right)' = \omega^0_{mn}, \tag{4.6}$$

and the solution can be expressed using ω^0_{mn} as

$$\omega^1_{mn}(\eta) = E^1\mathrm{e}^{-\Phi} + F^1\mathrm{e}^{-\Phi}\int_0^\eta \mathrm{e}^{\Phi(\eta')}\,\mathrm{d}\eta' + \mathrm{e}^{-\Phi}\int_0^\eta \mathrm{e}^{\Phi(\eta')}\int_0^{\eta'} \omega^0_{mn}(\eta'')\,\mathrm{d}\eta''\,\mathrm{d}\eta', \tag{4.7}$$

where Φ is defined as

$$\Phi(\eta) = \int_0^\eta \phi(\eta')\,\mathrm{d}\eta' \tag{4.8}$$

and E^0, E^1, F^0, F^1 are arbitrary constants. The higher-order terms can be computed similarly. The series expansion (4.3) is valid in the entire spatial domain from the wall to the inflow, but, as such, is of limited use because it involves unknown constants. In the next section, the exact solution of (4.1) in a region outside the Hiemenz boundary layer is obtained for arbitrary λ and σ_0. By examining the characteristics of the exact solution for the case of $\lambda \gg 1$ and $\sigma_0 \ll 1$, the unknown constants in (4.5) can be determined.

4.2. *Outside the boundary layer*

Outside the Hiemenz boundary layer, the relevant length and velocity scales are determined by the incoming disturbance. To facilitate the subsequent analysis, the vorticity equation (4.1) is first rescaled by l_d and u_d defined in (2.24)

$$\omega''_{mn} + \lambda\phi\omega'_{mn} + (\lambda\phi' - n^2 - \mathrm{i}\, m\lambda\sigma_0)\omega_{mn} = 0. \tag{4.9}$$

Note here both the dependent and independent variables are rescaled, and the derivatives are now with respect to the new independent variable $s = y^*/l_d = \eta/\sqrt{\lambda}$.

In particular, the mean velocity profile $\phi(s)$ in (4.9) is equal to the $\phi(\eta)$ multiplied by the factor $1/\sqrt{\lambda}$, i.e. $\phi(s) = \phi(\eta)/\sqrt{\lambda}$. The boundary conditions for the mean and disturbance flow remain unchanged under this rescaling.

As noted in figure 2, the mean velocity profile ϕ takes a simple irrotational form outside the Hiemenz boundary layer

$$\phi \sim s - s_d, \qquad \phi' \sim 1, \tag{4.10}$$

where s_d represents the displacement thickness δ_d of the Hiemenz boundary layer, i.e. $s_d = \delta_d/\sqrt{\lambda}$. In this region, the main effect of ϕ on the disturbances, besides the convection, is to stretch the ξ-component of the incoming vorticity. When the disturbance scale is relatively large, viscosity plays a less important role and the straining effect leads to an increase of the vorticity.

Denoting ω_{mn} outside the boundary layer by ω^p_{mn} and using (4.10), (4.9) becomes

$$\left(\omega^p_{mn}\right)'' + \lambda\,(s - s_d)\left(\omega^p_{mn}\right)' + (\lambda - n^2 - \mathrm{i}\,m\lambda\sigma_0)\omega^p_{mn} = 0. \tag{4.11}$$

On introducing a new independent variable τ

$$\tau = -\tfrac{1}{2}\lambda(s - s_d)^2, \tag{4.12}$$

the vorticity equation is further transformed into

$$\tau\left(\omega^p_{mn}\right)'' + \left(\tfrac{1}{2} - \tau\right)\left(\omega^p_{mn}\right)' - \frac{\left(\lambda - n^2 - \mathrm{i}m\lambda\sigma_0\right)}{2\lambda}\omega^p_{mn} = 0, \tag{4.13}$$

where $'$ stands for $\mathrm{d}/\mathrm{d}\tau$. This is the confluent hypergeometric equation of the general form

$$xy'' + (c - x)y' - ay = 0, \tag{4.14}$$

whose solution may be expressed as

$$y = C_1 M(a;\, c;\, x) + C_2\, U(c - a;\, c;\, -x)\,\mathrm{e}^x$$

for $c \neq 0, \pm 1, \pm 2 \cdots$. $M(a;c;x)$ and $U(a;c;x)$ are the first and second kind of confluent hypergeometric functions (Abramowitz & Stegun 1970). In the present case, they correspond to

$$y = \omega^p_{mn}; \qquad x = \tau; \qquad c = \tfrac{1}{2}; \quad a = \frac{\lambda - n^2 - \mathrm{i}m\lambda\sigma_0}{2\lambda}. \tag{4.15}$$

An integral representation for $M(a;c;x)$ when $\mathrm{Re}\,c > \mathrm{Re}\,a > 0$ is

$$M(a;\, c;\, x) = \frac{\Gamma(c)}{\Gamma(a)\Gamma(c - a)} \int_0^1 t^{a-1}(1 - t)^{c-a-1}\mathrm{e}^{xt}\,\mathrm{d}t$$

and $U(a;c;x)$ can be expressed by $M(a;c;x)$ through the following expression.

$$U(a;\, c;\, x) = \frac{\pi}{\sin(c\pi)}\left\{\frac{M(a;\, c;\, x)}{\Gamma(1 + a - c)\Gamma(c)} - x^{1-c}\frac{M(1 + a - c;\, 2 - b;\, x)}{\Gamma(a)\Gamma(2 - c)}\right\}. \tag{4.16}$$

Hence, the general solution for the vorticity becomes

$$\omega^p_{mn} = C_1\, M\left(\frac{\lambda - n^2}{2\lambda} - \mathrm{i}\,\frac{m\sigma_0}{2};\, \tfrac{1}{2};\, \tau\right) + C_2\, U\left(\frac{n^2}{2\lambda} + \mathrm{i}\,\frac{m\sigma_0}{2};\, \tfrac{1}{2};\, -\tau\right)\mathrm{e}^{\tau}. \tag{4.17}$$

For $\lambda < 1$, the solution simply decays from its upstream value, and for $\lambda = 1$ it

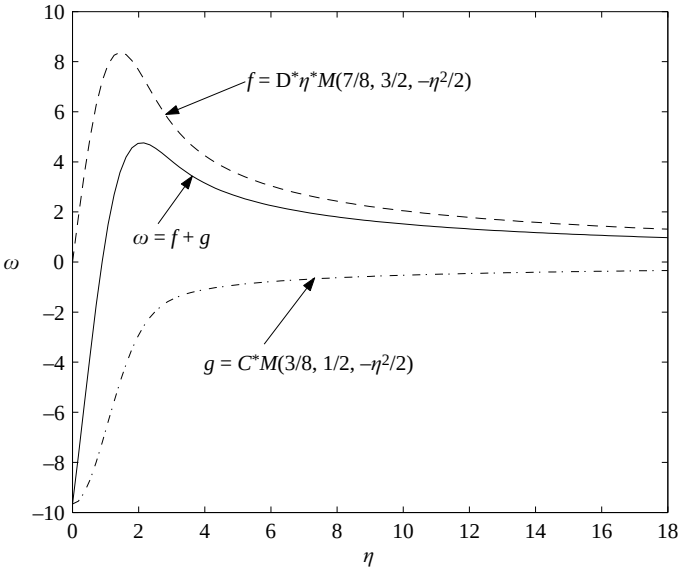

FIGURE 10. A typical vorticity profile composed of two confluent hypergeometric functions. $\lambda = 4$, $\sigma_0 = 0$.

becomes a constant. So, in what follows, only the case of $\lambda > 1$ is considered. First, writing s in terms of the original variable η, and by the definition of τ, it follows that

$$\eta = \sqrt{\lambda}s\,, \qquad \tau = -\frac{(\eta - \delta_d)^2}{2} = -\frac{\tilde{\eta}^2}{2}, \tag{4.18}$$

where the shifted coordinate $\tilde{\eta}$ is defined as

$$\tilde{\eta} = \eta - \delta_d. \tag{4.19}$$

After some simplification, the general solution for the vorticity outside the boundary layer ω^p_{mn} may be expressed as

$$\omega^p_{mn} = C_{mn}\, M\left(\frac{\lambda - n^2}{2\lambda} - \mathrm{i}\,\frac{m\sigma_0}{2};\, \tfrac{1}{2};\, -\frac{\tilde{\eta}^2}{2}\right) + D_{mn}\, M\left(\frac{2\lambda - n^2}{2\lambda} - \mathrm{i}\,\frac{m\sigma_0}{2};\, \tfrac{3}{2};\, -\frac{\tilde{\eta}^2}{2}\right)\tilde{\eta}, \tag{4.20}$$

where C_{mn}, D_{mn} are arbitrary constants. A typical solution for $\lambda = 4$, $\sigma_0 = 0$ composed of two confluent hypergeometric functions (with C_{mn}, D_{mn} specified by (4.35) in § 4.4) is illustrated in figure 10.

4.3. *Composite solution*

To facilitate further analysis, the series solutions (4.3)–(4.7) is combined with the solution outside the boundary layer to derive a composite asymptotic solution. To do so, the unknown coefficients in the series expansion must be determined first. Notice that as $\eta \to \infty$,

$$\phi \sim \tilde{\eta}, \qquad \Phi \sim \Phi_0 + \frac{\tilde{\eta}^2}{2}, \tag{4.21}$$

where $\Phi_0 = \int_0^\infty (\phi - \tilde{\eta})\,\mathrm{d}\eta - \delta_d^2/2$ is an integral constant. This asymptotic representation is valid for $\tilde{\eta} > \tilde{\eta}_0$, where $\tilde{\eta}_0 \geqslant \delta_d$ is a location beyond which the irrotational flow

applies. The zeroth-order series solution (4.5) may be rewritten as

$$\omega^0_{mn}(\eta) = \mathrm{e}^{-\Phi}\left[E^0 + F^0\int_0^{\eta_0}\mathrm{e}^{\Phi(\eta')}\,\mathrm{d}\eta'\right] + F^0\,\mathrm{e}^{-\Phi}\int_{\eta_0}^{\eta}\mathrm{e}^{\Phi(\eta')}\,\mathrm{d}\eta'. \tag{4.22}$$

However when $\eta \to \infty$, the first term in (4.22) vanishes, so it follows that

$$\omega^0_{mn}(\eta) \sim F^0\exp(-\Phi)\int_{\eta_0}^{\eta}\exp(\Phi(\eta'))\,\mathrm{d}\eta' \sim F^0\exp(-\tilde{\eta}^2/2)\int_0^{\tilde{\eta}}\exp(\tilde{\eta}'^2/2)\,\mathrm{d}\tilde{\eta}', \tag{4.23}$$

where in the second expression, (4.21) has been used and the lower limit has been extended to zero using the same decomposition as in (4.22). On the other hand, the corresponding zeroth-order expansion of (4.20) in ϵ becomes

$$\omega^{p0}_{mn} = C_{mn}\,M\left(\tfrac{1}{2};\tfrac{1}{2};\,-\tfrac{1}{2}\tilde{\eta}^2\right) + D_{mn}\,M\left(1;\tfrac{3}{2};\,-\tfrac{1}{2}\tilde{\eta}^2\right)\tilde{\eta}. \tag{4.24}$$

Noting the following identities

$$M(a;a;z) = \exp z, \qquad \exp(-z^2/2)\int_0^z \exp(z'^2/2)\,\mathrm{d}z' = zM\left(1;\tfrac{3}{2};-\tfrac{1}{2}z^2\right) \tag{4.25}$$

and comparing (4.23) and (4.24) for large η, we obtain

$$D_{mn} = F^0, \tag{4.26}$$

since the first term in (4.24) vanishes more rapidly than the second.

No appropriate matching condition for C_{mn} can be derived from the large η asymptotics. Hence, it is necessary to find the matching condition by considering the behaviour of the vorticity close to the wall. As shown in figure 9, the wall vorticity plays a key role in determining the interaction between the incoming disturbances and the Hiemenz boundary layer. An initial choice for matching C_{mn} and E^0 therefore seems to require the wall vorticity obtained from (4.20) and (4.5) to be equal. However, the vorticity at the wall obtained by setting $\eta = 0$ in (4.20) is not accurate, since (4.20) is only applicable outside the Hiemenz boundary layer. A more appropriate choice is to require the vorticity obtained from the two solutions to match at the edge of the Hiemenz boundary layer where both solutions apply. This results in the following expression for C_{mn},

$$C_{mn} = \left[E^0 + F^0\int_0^{\delta}\exp(\Phi)\,\mathrm{d}\eta\right]\exp(-\Phi_\delta) - F^0\int_0^{\delta-\delta_d}\exp(\eta^2/2)\,\mathrm{d}\eta, \tag{4.27}$$

where $\Phi_\delta = \Phi(\delta) - (\delta-\delta_d)^2/2$. Further matching (4.20) to (4.7) at higher order requires evaluation of $M(a,c,z)$ subject to the perturbation of a and the asymptotic behaviour of the last term in (4.7) for large η, for which the explicit expressions have not been obtained. Nevertheless, an approximate solution of ω_{mn}, more explicit than the series expansion, can still be constructed by a similar procedure to those in matched asymptotics (Van Dyke 1975), i.e.

$$\omega_{mn} \sim \omega^0_{mn} + \omega^p_{mn} - \omega^{p0}_{mn}, \tag{4.28}$$

here the expressions for ω^0_{mn}, ω^p_{mn} and ω^{p0}_{mn} are (4.5), (4.20) and (4.24), respectively. Using the matching condition (4.26) and (4.27), we obtain the following asymptotic expression for the incoming vorticity in the case of $\lambda \gg 1$ and $\sigma_0 \ll 1$ in the whole

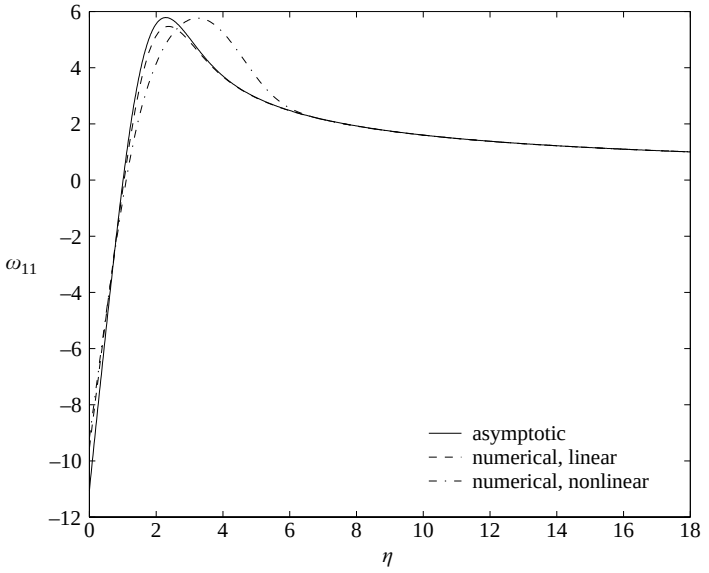

FIGURE 11. Comparison of vorticity profile between numerical and asymptotic solutions at $\lambda = 4$.

range of η

$$\omega_{mn}(\eta) \sim C_{mn}\left[M\left(\frac{\lambda - n^2}{2\lambda} - \mathrm{i}\,\frac{m\sigma_0}{2}; \tfrac{1}{2}; -\frac{(\eta-\delta_d)^2}{2}\right) + \exp(\Phi_\delta - \Phi) - \exp(-(\eta-\delta_d)^2/2)\right]$$
$$+ D_{mn}\left[M\left(\frac{2\lambda - n^2}{2\lambda} - \mathrm{i}\,\frac{m\sigma_0}{2}; \tfrac{3}{2}; -\frac{(\eta-\delta_d)^2}{2}\right)(\eta-\delta_d)\right.$$
$$+ \exp(\Phi_\delta - \Phi)\int_0^{\delta-\delta_d} \exp(\eta^2/2)\,\mathrm{d}\eta + \exp(-\Phi)\int_\delta^\eta \exp(\Phi(\eta'))\,\mathrm{d}\eta'$$
$$\left. - M\left(1; \tfrac{3}{2}; -\frac{(\eta-\delta_d)^2}{2}\right)(\eta-\delta_d)\right]. \tag{4.29}$$

Here, the dependence of ω_{mn} as an explicit function of λ and σ_0, not readily obtained by the series expansion itself, has been retained in (4.29), and by correcting the ω_{mn}^{p0} in the near-wall region through ω_{mn}^0, (4.29) also extends inside the Hiemenz boundary layer. In figures 11 and 12, the comparisons between the composite asymptotic solution (4.29) and the numerical solution are shown for $\lambda = 4$ and $\lambda = 36$, respectively. The vorticity profiles have been normalized by its value at the inflow boundary $\eta = H_0$. The numerical solutions are obtained by solving both the linear equation (4.9) and the fully nonlinear equation (2.16). The asymptotic solution and the linear numerical solution agree well at $\lambda = 4$ and become indistinguishable at $\lambda = 36$. Recall that the disturbance amplitude is here taken as 10% of the mean free-stream velocity, $A_p = 0.1\phi(H_0)$, and the linear solution approaches the nonlinear solution quite well as λ increases. This indicates that the present linear analysis is adequate for describing the characteristics of disturbance development in a Hiemenz flow.

4.4. *Boundary conditions for the vorticity*

The general composite solution in (4.29) describes the evolution of disturbance vorticity in the whole domain from the inflow to the wall boundary. Now, we set out to specify the constants C_{mn} and D_{mn} by the inflow and wall boundary conditions. In

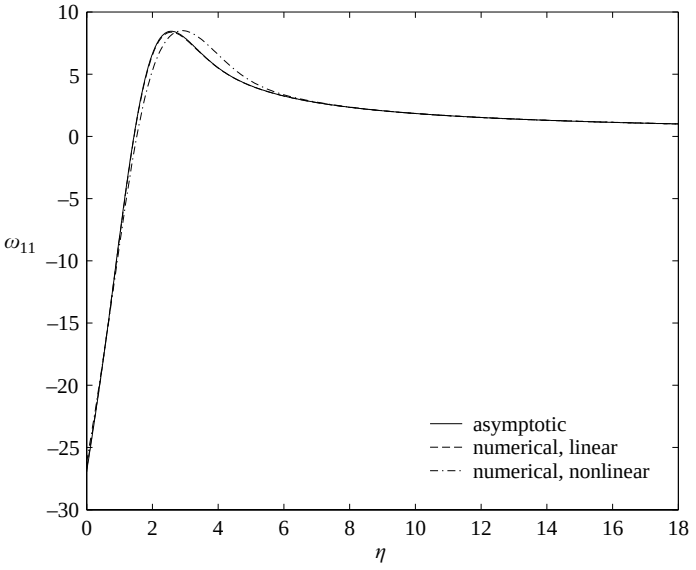

FIGURE 12. Comparison of vorticity profile between numerical and asymptotic solutions. $\lambda = 36$.

fact, it will later become clear that both C_{mn} and D_{mn} have clearly defined physical meanings. First, the initial disturbance vorticity is introduced at the inflow boundary far upstream, i.e.

$$\omega_{mn} = \omega_{mn}(H_0) \qquad \text{at} \qquad \eta = H_0. \tag{4.30}$$

Then, the value of vorticity at the wall must be specified. However, there is no explicit expression for $\omega_{mn}(\eta = 0)$ because, as indicated by Sutera (1965), the vorticity equation is coupled, through the no-slip boundary condition, with the velocity equations. To obtain the correct value of vorticity on the wall, the equation for normal velocity v_{mn} must be solved first. By (2.13) and (2.14), it follows

$$v''_{mn} - n^2 k_0^2 v_{mn} = -\mathrm{i}nk_0\omega_{mn} - u'_{mn} \quad \text{with} \quad v_{mn}(0) = v'_{mn}(0) = 0. \tag{4.31}$$

Using the method of variation of parameters, the solution of v_{mn} satisfying the above boundary conditions is

$$v_{mn} = -\frac{\exp(nk_0\eta)}{2}\int_0^\eta (\mathrm{i}\omega_{mn} + u_{mn})\exp(-nk_0\eta')\,\mathrm{d}\eta' + \frac{\exp(-nk_0\eta)}{2}\int_0^\eta (\mathrm{i}\omega_{mn} - u_{mn})\exp(nk_0\eta')\,\mathrm{d}\eta'. \tag{4.32}$$

However, (4.32) contains u_{mn} which couples with v_{mn} through (2.15) and has not been solved. Nevertheless, by requiring that v_{mn} is bounded as $\eta \to \infty$, further analysis (see Appendix A) shows that the second boundary condition for ω_{mn} can be expressed as

$$\int_0^\infty \omega^p_{mn}\exp(-nk_0\eta)\,\mathrm{d}\eta = 0. \tag{4.33}$$

Together with (4.30), we now have

$$M_1 C_{mn} + M_2 D_{mn} = 1, \tag{4.34a}$$

$$I_1 C_{mn} + I_2 D_{mn} = 0. \tag{4.34b}$$

Solving (4.34) for C_{mn} and D_{mn} yields

$$C_{mn} = -\frac{I_2}{M_2 I_1 - M_1 I_2}, \qquad D_{mn} = \frac{I_1}{M_2 I_1 - M_1 I_2}, \tag{4.35}$$

where

$$M_1 = M\left(\frac{\lambda - n^2}{2\lambda} - \mathrm{i}\frac{m\sigma_0}{2}; \tfrac{1}{2}; -\frac{(H_0 - \delta_d)^2}{2}\right), \tag{4.36a}$$

$$M_2 = M\left(\frac{2\lambda - n^2}{2\lambda} - \mathrm{i}\frac{m\sigma_0}{2}; \tfrac{3}{2}; -\frac{(H_0 - \delta_d)^2}{2}\right)(H_0 - \delta_d), \tag{4.36b}$$

$$I_1 = \int_0^\infty M\left(\frac{\lambda - n^2}{2\lambda} - \mathrm{i}\frac{m\sigma_0}{2}; \tfrac{1}{2}; -\frac{(\eta - \delta_d)^2}{2}\right)\exp(-nk_0\eta)\,\mathrm{d}\eta, \tag{4.36c}$$

$$I_2 = \int_0^\infty M\left(\frac{2\lambda - n^2}{2\lambda} - \mathrm{i}\frac{m\sigma_0}{2}; \tfrac{3}{2}; -\frac{(\eta - \delta_d)^2}{2}\right)(\eta - \delta_d)\,\exp(-nk_0\eta)\,\mathrm{d}\eta. \tag{4.36d}$$

Notice that in (4.34) the vorticity at the inflow has been chosen as $\omega_{mn}(H_0) = 1$ since the equation is linear. The value of ω_{mn} therefore represents the factor by which the initial vorticity is amplified or attenuated as it approaches the wall. Before we discuss the asymptotic behaviours of C_{mn} and D_{mn}, a few remarks on their significance and qualitative behaviour are in order. First, (4.29) indicates that for a vortical disturbance specified upstream by λ and σ_0, the induced vorticity on the wall is directly related to the values of C_{mn} and D_{mn}. In the case of $\lambda \gg n^2$, $|C_{mn}|$ represents the amplitude of vorticity at the wall, i.e. $|\omega_{mn}(0)| \sim |C_{mn}|$, and D_{mn} represents the amplitude of the normal derivative of the vorticity at the wall, i.e. $|\omega'_{mn}(0)| \sim |D_{mn}|$. This can also be seen more clearly from figure 10. Consequently, the amplitudes of C_{mn} and D_{mn} indicate the effectiveness of the disturbance in penetrating the boundary layer and modifying the mean flow structures near the wall. Secondly, the boundary condition (4.33) shows that for steady disturbance, ω^p must change sign in the flow domain; vorticity with sign opposite to the incoming vorticity must be developed at the wall in order to satisfy the no-slip boundary condition. This can be observed clearly from the vorticity contours in figure 6. Note that the amplitude of the induced vorticity at the wall $\omega_{mn}(0)$, as shown in figure 9, approaches a constant when λ becomes large. The origin and implications of this behaviour of $\omega_{mn}(0)$ can be understood through the asymptotic analysis for large λ and small σ_0, and is presented in the next section.

5. Asymptotic behaviour

In this section, the asymptotic behaviour of C_{mn} and D_{mn} in the vorticity expression is analysed for the large-scale $\lambda \gg 1$ and low-frequency $\sigma_0 \ll 1$ disturbances. Based on this analysis, a scaling relation for the heat transfer enhancement in stagnation-point flows in the presence of upstream disturbances is also derived.

5.1. *Vorticity asymptotes*

The asymptotic expression of C_{mn} for large λ and small σ_0 may be obtained as (see the Appendix B)

$$|C_{mn}| \sim H_0\left[1 + (a_1 - \ln H_0)\frac{n^2}{\lambda}\right]\left[1 - \frac{\alpha_n m^2}{8}\sigma_0^2\right], \tag{5.1}$$

where $a_1 = (\ln 2 + \gamma)/2$ and $\gamma = 0.5772156\cdots$ is the Euler constant. The expression for $|D_{mn}|$ can be similarly obtained.

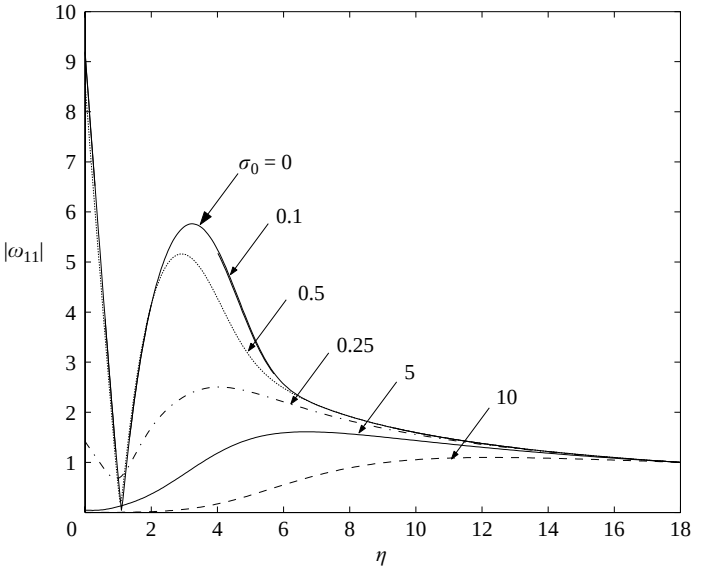

FIGURE 13. Vorticity profiles for different fundamental disturbance frequency σ_0 at $\lambda = 4$.

An important observation for (5.1) is that the amplitude of the vorticity induced at the wall, up to the leading order, is linearly dependent on the normal distance H_0 between the wall and the upstream location where the disturbance is introduced. This means that for large λ and small σ_0, within the linear dynamics regime, the amplification factor due to the vortex stretching for the initial vortical disturbance has an upper limit set by H_0. This explains the behaviour seen in figure 9 as λ becomes large. From (5.1), we also find that the unsteadiness of the disturbances tends to decrease the induced vorticity amplitude at the wall compared with the steady case, but only to the second order in terms of frequency σ_0. In figure 13, the vorticity profiles at different frequencies are computed numerically for $\lambda = 4$ to show the effect of the disturbance unsteadiness. Notice that although the numerical computation uses the full nonlinear equations, the vorticity value at the wall indeed follows the asymptotic behaviour (5.1) and shows only modest changes relative to the steady case for $\sigma_0 < 0.5$. When we consider time scale, $\sigma_0 \ll 1$ implies that the disturbance turnover time is much longer than the time scale of mean flow distortion; vortex stretching is predominant, and hence flow structures similar to the steady case are generated. For the high-frequency case $\sigma_0 \gg 1$, (4.2) is not valid, and in the course of disturbances being convected towards the wall, many cycles of oscillation have been completed. The net vorticity induced at the wall is small because of the cancellation effect of the incoming disturbance vorticity with alternating signs. This effect, also known as 'vortex piling', has been analysed by Hunt (1973). Our numerical results in figure 13 show that, indeed, the induced vorticity at the wall decays monotonically with σ_0 and becomes rather small when $\sigma_0 > 2.5$.

5.2. *Heat transfer scaling*

With the amplitude of the velocity disturbance at the inflow $v_{mn}(H_0)$ kept constant, the vorticity ω_{mn} introduced at the inflow varies as a function of λ

$$\omega_{mn}(H_0, \lambda) = \omega_{mn}(H_0, 1)\lambda^{-1/2}, \tag{5.2}$$

where $\omega_{mn}(H_0, 1)$ is a reference value of vorticity for $\lambda = 1$. Recall that, C_{mn}, D_{mn}, as functions of λ and σ_0, represent the amplification factor for the wall vorticity value. The amplification factor increases with λ, initially at a large rate, but eventually it approaches a constant value determined by H_0. Together with the $\lambda^{-1/2}$ factor, this gives rise to an overall optimum amplification for $\lambda \approx 4$.

Once the vorticity is obtained, the corresponding velocity disturbance can be found by (4.32) as

$$v_{mn} = \tfrac{1}{2}\exp(-nk_0\eta)\int_0^{\eta}(\mathrm{i}\omega_{mn} - u_{mn})\exp(nk_0\eta')\,\mathrm{d}\eta. \tag{5.3}$$

As shown in Appendix A, the second term of the integrand in (5.3) is expected to be much smaller than the first for $k_0 \ll 1$. Hence, the dependence of v_{mn} on λ directly follows that of ω_{mn}. When λ is large, the vorticity amplification factor C_{mn} approaches a constant. Accordingly, $|v|_{max} \sim \lambda^{-1/2}$, a trend noted in figure 8. Now from (2.23), it follows that

$$\frac{\Delta h}{h} = \frac{\theta_0'(0)}{\Theta'(0)} \sim \sum_{m,n} |v_{mn}|\,|\theta_{mn}|. \tag{5.4}$$

For the temperature disturbance θ_{mn}, the linearized equation of (2.17) is

$$\theta_{mn}'' + Pr\phi\theta_{mn}' - (n^2k_0^2 + \mathrm{i}m\,Pr\sigma_0)\theta_{mn} = Pr\,v_{mn}\Theta'. \tag{5.5}$$

The amplitude of the temperature fluctuation θ_{mn} can be deduced; that is, θ_{mn} will be proportional to the amplitude v_{mn} and follows the same asymptotic dependence on λ as ω_{mn} and v_{mn}. Hence, we have

$$|v_{mn}(\eta)| \sim |\theta_{mn}(\eta)| \sim |\omega_{mn}(\eta)| \sim |C_{mn}|\frac{|v_{mn}(H_0)|}{\sqrt{\lambda}}. \tag{5.6}$$

For the low-frequency case $\sigma_0 \ll 1$, the heat transfer enhancement scales with the disturbance parameters,

$$\frac{\Delta h}{h} \sim \frac{A_p^2 H_0^2}{\lambda}\sum_{m,n}\left[1 + (a_1 - \ln H_0)\frac{n^2}{\lambda}\right]^2\left[1 - \frac{\alpha_n}{8}m^2\sigma_0^2\right]^2 |v_{mn}(H_0)|^2. \tag{5.7}$$

When $\lambda \gg 1$, we have $\Delta h/h \sim \lambda^{-1}$ for fixed A_p, a behaviour noted in figure 8. We can rewrite $1/\lambda$ in terms of the disturbance length scale l_d, and obtain the following scaling relation for the relative heat transfer enhancement at low disturbance frequency

$$\frac{\Delta h}{h} \sim \frac{A_p^2}{l_d^2}\sum_{m,n}\left(1 - \frac{\alpha_n}{8}m^2\sigma_0^2\right)^2 |v_{mn}(H_0)|^2. \tag{5.8}$$

The above expression reveals different roles played by the various flow parameters in heat transfer enhancement. First, the enhancement is proportional to the square of the disturbance amplitude A_p owing to the net convective flux by the disturbance modes. Secondly, the length scale of the disturbance has a critical effect upon the heat transfer enhancement. For large-scale disturbances, the heat transfer enhancement decreases with increased length scale. The most effective disturbance will be those with length scales comparable to the boundary-layer thickness. Finally, the overall effect of the frequency of the disturbances is to reduce the heat transfer enhancement. The decrease is of the second order when the frequency is low, and at high frequencies the heat transfer enhancement approaches to zero owing to the rapid decay of the incoming disturbances. So far, the Prandtl number has been kept at a constant in the

analysis $Pr = 0.71$. For a different Prandtl number, both the mean thermal boundary-layer thickness and the amplitude of θ_{mn} will be affected. Nevertheless, the qualitative dependence on Prandtl number can be inferred from (2.23). For small Pr, the $\Delta h/h$ increases with the increase of Pr, but as Pr becomes very large, the effect diminishes owing to the extremely thin thermal boundary layer. So there will be an optimal value of Prandtl number for each fixed value of λ which gives the maximum heat transfer enhancement. Numerical calculations show that this optimal Prandtl number decreases with increasing λ from $Pr = 7$ at $\lambda = 1.5$ to $Pr = 0.71$ at $\lambda = 12$. However, for a fixed Prandtl number, the optimal value of λ is still around $\lambda = 4$, and the overall maximum value of $\Delta h/h$ occurs around $\lambda = 4$ and $Pr = 1.5$.

6. Discussion of free-stream turbulence

One of the primary goals of the present analysis is to gain improved understanding of the effect of free-stream turbulence in stagnation-point flows. In this section, we derive a scaling correlation between the heat transfer enhancement and the characteristics of the free-stream turbulence based on the preceding analysis. The formulation is analogous to that in RDT, i.e. the overall changes of the turbulence statistics are obtained by integrating over all the Fourier modes once the modal distortion for each of them is known. The comparison between the scaling correlation and experimental measurements serves as a test of the applicability of the present analysis to relevant engineering problems.

The free-stream turbulence is assumed to be isotropic and homogeneous. On expressing the velocity fluctuations as

$$\boldsymbol{u}(\xi, \eta, \zeta, t) = \int\int\int_{-\infty}^{\infty} \hat{\boldsymbol{u}}(\kappa_1, \kappa_2, \kappa_3) \exp\left[\mathrm{i}(\kappa_1\xi + \kappa_2\eta + \kappa_3\zeta + \sigma t)\right] \mathrm{d}\kappa_1\, \mathrm{d}\kappa_2\, \mathrm{d}\kappa_3, \quad (6.1)$$

and using the frozen-turbulence approximation, the free-stream turbulence is convected into the domain through the inflow boundary with a time frequency $\sigma = -U\kappa_2$. Let $\eta = H_0$ be the location of the inflow boundary, then

$$\boldsymbol{u}(\xi, H_0 - Ut, \zeta) = \int\int\int_{-\infty}^{\infty} \hat{\boldsymbol{u}}_{in}(\kappa_1, \kappa_2, \kappa_3) \exp\left(\mathrm{i}(\kappa_1\xi + \kappa_2(H_0 - Ut) + \kappa_3\zeta)\right) \mathrm{d}\kappa_1\, \mathrm{d}\kappa_2\, \mathrm{d}\kappa_3. \quad (6.2)$$

While being convected towards the stagnation point, the free-stream turbulence experiences an accumulated vortex stretching in the ξ-direction by the diverging mean flow. As a result, this leads to $k_1 \ll k_2, k_3$ in the stagnation-point region. Thus, the dependence of $\boldsymbol{u}$ on ξ may be neglected in the above expression, and the inverse transformation of $\hat{\boldsymbol{u}}_{in}$ is now written as

$$\hat{\boldsymbol{u}}_{in}(\kappa_2, \kappa_3) = \frac{1}{(2\pi)^2} \int\int_{-\infty}^{\infty} \boldsymbol{u}(H_0 - Ut, \zeta) \exp\left(-\mathrm{i}(\kappa_2(H_0 - Ut) + \kappa_3\zeta)\right) \mathrm{d}\zeta\, \mathrm{d}t \quad (6.3)$$

The heat transfer enhancement in the presence of free-stream turbulence can be computed in terms of the downstream velocity and temperature spectra $\hat{\boldsymbol{u}}(\eta, \kappa_2, \kappa_3)$, $\hat{\theta}(\eta, \kappa_2, \kappa_3)$. Following the discussion in preceding sections, we assume that for the η-velocity $\hat{v}$ and temperature $\hat{\theta}$

$$\hat{v}(\eta, \kappa_2, \kappa_3) = G(\eta)\hat{v}(H_0, \kappa_2, \kappa_3) \sim \hat{\theta}(\eta, \kappa_2, \kappa_3), \quad (6.4)$$

where function $G(\eta)$ represents the amplification ratio at downstream location η for mode $\hat{v}(\kappa_2, \kappa_3)$ owing to mean flow straining and viscous dissipation. Taking the

amplitude of $G(\eta)$ as $C(\kappa_2, \kappa_3)$, i.e.

$$|G(\eta, \kappa_2, \kappa_3)| \sim |C(\kappa_2, \kappa_3)|, \tag{6.5}$$

the overall effect of free-stream turbulence on the heat transfer can be estimated by summing the contribution from all the modes of different wavenumbers and frequencies. In view of (2.23), for a single-mode disturbance specified at the inflow, the heat transfer enhancement mainly results from the second-order interaction terms. Thus, in the present linear analysis, when (2.23) and (6.4) are used to find the contribution from mode $\hat{v}_{mn}$, the nonlinear term $\mathcal{N}_4$ can be written as

$$\mathcal{N}_4(\kappa_2, \kappa_3) \sim |C(\kappa_2, \kappa_3)|^2 \, |\hat{v}(\kappa_2, \kappa_3)|^2 \sim |C(\kappa_2, \kappa_3)|^2 \Phi_{ii}(\kappa_2, \kappa_3), \tag{6.6}$$

where the $\Phi_{ii}(\kappa_2, \kappa_3)$ is the energy spectra density for the free-stream turbulence. Since the free-stream turbulence is assumed to be isotropic and homogeneous, the energy spectrum $E(\kappa)$ is defined as:

$$E(\kappa) = 2\pi \Phi_{ii}(\kappa) \kappa^2. \tag{6.7}$$

The turbulence intensity T_u and the integral length scale L may be related to the amplitude and fundamental wavenumber of energy containing range by

$$A_p^2 \sim (U \, T_u)^2, \quad \kappa_0 \sim \frac{1}{L}. \tag{6.8}$$

The total contribution from all wavenumber components is the integration of the turbulent energy spectrum, i.e.

$$A_p^2 \sum_{\kappa_2, \kappa 3} |\hat{v}(H_0, \kappa_2, \kappa_3)|^2 \sim \int\int\int_0^\infty \Phi_{ii}(\kappa) \, \mathrm{d}^3\kappa \sim T_u^2 \int_0^\infty \frac{E(\kappa)}{q^2 L} \, \mathrm{d}(\kappa L). \tag{6.9}$$

After substitution of (6.6) and (6.9) into the expression for heat transfer enhancement (2.23), it becomes

$$\frac{\Delta h_T}{h} \sim T_u^2 \int \tilde{E}(\kappa L) \, |C(kL)|^2 \, \mathrm{d}(\kappa L), \tag{6.10}$$

where $\tilde{E}(\kappa L) = E(\kappa)/(q^2 L)$. In most of the engineering problems involving turbulence impinging on a stagnation point, the turbulent eddy turnover time is typically much longer than the time scale associated with the mean flow straining, i.e. $\sigma_0 \ll 1$. In addition, the turbulence length scale is assumed to be much larger than the boundary-layer thickness, i.e. $L \gg \delta$. By (5.6), for a fixed upstream location it follows that

$$|C(\kappa L)| \sim \frac{C_{mn}}{\sqrt{\lambda}} \sim \frac{D}{l_d} \sim (\kappa L)\left(\frac{D}{L}\right) \quad \text{for} \quad 0 < \kappa < \kappa_{max}. \tag{6.11}$$

Hence,

$$\frac{\Delta h_T}{h} \sim \left(\frac{D \, T_u}{L}\right)^2 \int_0^{\kappa_{max} L} \tilde{E}(\kappa L) \, (\kappa L)^2 \, \mathrm{d}(\kappa L), \tag{6.12}$$

where k_{max} represents the highest wavenumber component having a contribution to the heat transfer augmentation. From the previous analysis, the heat transfer enhancement reaches its maximum value with the disturbance scale similar to the boundary-layer thickness. At even smaller scales, the disturbances decay rapidly because of the viscous dissipation and have little effect on the wall quantities.

For practical engineering problems, such as flows over a bluff body, the boundary-layer thickness at the stagnation region scales as

$$l_0 = \sqrt{\nu^*/A^*} \sim \delta \sim \frac{D}{\sqrt{Re}}, \tag{6.13}$$

where the Reynolds number is based on the mean flow U and the diameter of curvature D (see figure 1*a*). For an effective strain rate A^*, e.g. $A^* = 4U/D$ for a circular cylinder, κ_{max} may be expressed as

$$\kappa_{max} L \sim \frac{L}{\delta} \sim \sqrt{Re}\frac{L}{D}. \tag{6.14}$$

Furthermore, the energy spectrum of the free-stream turbulence is assumed to follow the Kolmogoroff $-5/3$ law

$$\tilde{E}(\kappa L) \sim (\kappa L)^{-5/3}. \tag{6.15}$$

Substituting (6.14) and (6.15) into (6.12), the heat transfer enhancement at stagnation point can now be correlated to the free-stream turbulence parameters by

$$\frac{\Delta h_T}{h} \sim \mathscr{H} = \frac{T_u^2 Re^{2/3}}{(L/D)^{2/3}}. \tag{6.16}$$

Note that here the three-dimensional spectrum function is used. Following the form of organized disturbances in previous discussion, a one-dimensional spectra is probably more appropriate. However, at high Reynolds number, it also follows the same $-5/3$ law as the three-dimensional spectrum.

In order to examine heat transfer scaling, (6.16) is compared against the experimental measurements for stagnation-point flows in the presence of free-stream turbulence. A recent experiment was conducted by Ames, Wang & Barbot (2002), in which the heat transfer to a model vane is measured for six different inlet turbulence conditions with turbulence intensity up to 14%. The different characteristics of the free-stream turbulence are generated using mesh biplanar grid and various mock combustion system configurations. The experimental set-up is representative to modern dry low NOx and aeroderivative combustors. The downstream vane heat transfer measurements can serve as a database for the validation of predictive methods. Another reason to choose this experiment is that the characteristics of free-stream turbulence, i.e. intensity and length scale, are measured with the model vane present in the flow. Thus, the mean velocity follows the Hiemenz profile at the locations where the turbulence is measured. This is the same case as has been assumed in the present analysis. In some other experiments (e.g. Van Fossen *et al.* 1995), the free-stream turbulence is first measured in the uniform flow without the model. When the model is present, the turbulence characteristics are obtained by extrapolation using a power law for decaying turbulence. At locations close to the stagnation point, the turbulence characteristics obtained by this method will be significantly different from those obtained with the presence of the model. Although the difference becomes smaller beyond a distance of the order of D away from the wall, the Hiemenz flow, as a good approximation at the stagnation point for bluff-body flows, is also only valid within the order of D away from the wall. Hence, in figure 14 the present heat transfer correlation is compared with the measurement of Ames *et al.* (2002) at four high-turbulence levels generated by grid as well as by aero-derivative and dry low NOx mock combustor system. The Reynolds number based on the leading-edge diameter ranges from 58 000 to 232 000; turbulence integral scale from $0.11D$

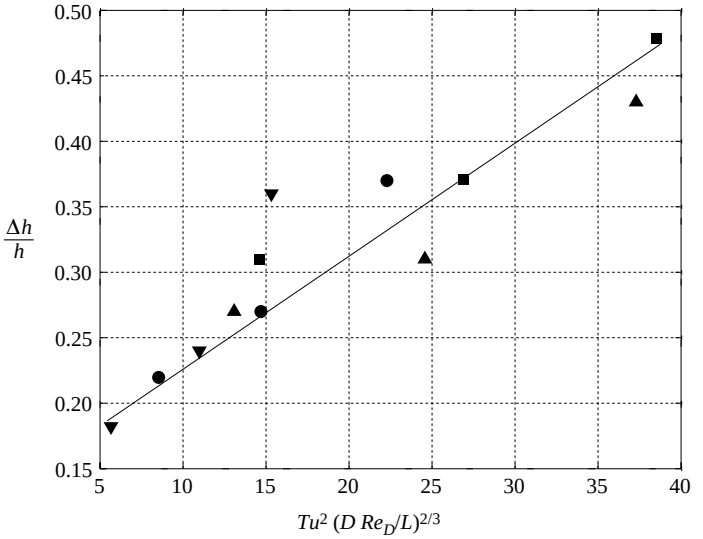

FIGURE 14. Experimental data of leading-edge heat transfer enhancement under free-stream turbulence correlated by the present scaling parameter $\mathscr{H}$. ●, grid; ■, aero-derivative; ▼, aero-derivative II; ▲, dry low NOx.

to $1.0D$ and the turbulence intensity from 8 to 14%. The collective experimental uncertainty is $\pm 5\%$ for turbulence measurement and $\pm 3\%$ for heat transfer data. Although some scatter is present, the correlation appears to agree reasonably well with the experimental data for the correlation parameter $\mathscr{H}$ over the range 5 to 35. Notice that the turbulence levels in these experiments are quite high, but the analysis indicates that only small-scale components contribute effectively to the heat transfer enhancement. So even if the total turbulence level is high, the amplitude at the small scale, i.e. the scale of boundary-layer thickness that affects the heat transfer most, would still be relatively small. For a single-mode velocity disturbance at a level equivalent to 10% of the mean flow, the numerical results show that the disturbance evolution can still be largely described by linear vortex dynamics. This may explain why the correlation based on linear analysis seems to hold even for the case of high turbulence intensity. Also, note that the present correlating parameter is close to the square of the empirical TLR parameter $TLR = T_u Re_D^{5/12}(D/L_u)^{1/3}$ proposed by Ames (1997), if the turbulence integral length scale were replaced by the 'energy scale' $Lu = 1.5|u'|^3/\epsilon_T$, where $|u'|$ is the r.m.s. streamwise fluctuation velocity and ϵ_T is the turbulent dissipation rate.

7. Conclusion

In this paper, the distortion of the unsteady three-dimensional disturbances in a Hiemenz boundary-layer flow and its effect on the wall heat transfer is analysed. By using the linearized disturbance equations, it is found that the vorticity outside the boundary layer can be expressed analytically in terms of confluent hypergeometrical functions, parameterized by the disturbance length scale and temporal frequency. When the scale of the disturbance is large and the frequency is low, an approximate asymptotic solution is obtained with explicit dependence on the disturbance length scale and frequency. This solution compares well with the full nonlinear numerical

solutions over a wide range of disturbance parameters. It is further shown that the ratio between the disturbance length scale and the boundary-layer thickness is the critical parameter in determining the amplification factor of the incoming vorticity, and represents the interaction between vortex stretching and viscous diffusion. The amplification factor is found to be inversely proportional to the length scale except at very small scales where it increases with increased length scale. The amplification is maximum value for a disturbance length scale about five times the Hiemenz boundary-layer thickness. The associated heat transfer enhancement also strongly depends on the disturbance length scale and is analysed through the induced vorticity at the wall. Compared to the steady case, the heat transfer enhancement is reduced by the unsteadiness of the disturbance, but the effect is of second order when the frequency is low. The analysis is further extended to the case of homogeneous and isotropic free-stream turbulence. The turbulence energy spectrum is assumed to follow the Kolmogoroff $-5/3$ law and the integral scale is much larger than the boundary-layer thickness. Under these conditions, a new scaling correlation is derived between the heat transfer enhancement and the turbulence intensity, integral length scale and the mean flow Reynolds number. In comparison to the recent experimental data on turbine blade heat transfer in the presence of free-stream turbulence, the present correlation provides a reasonable guide to the observed variations.

This work is supported by the Air Force Office of Scientific Research under grant no. F49620-01-1-0138 with Dr Tom Beutner as the programme manager. The computer resource was provided by the 48-node computer cluster under DoD DURIP grant no. F49620-01-1-0239. The authors thank the referees for their comments on the original draft of the paper.

Appendix A. Vorticity boundary conditions

Here, we derive the second boundary condition (4.33) for the vorticity ω_{mn}. For simplicity, the subscript mn will be dropped from the disturbance quantities. Hence, the linearized governing equations for ω, u and v can be written in a general form as

$$\mathscr{L}_{\omega}(\phi, \omega) = 0, \quad \mathscr{L}_{u}(\phi, v, u) = 0, \quad \mathscr{L}_{v}(u, \omega, v) = 0, \tag{A 1}$$

where the expressions for the $\mathscr{L}$ terms are those in (2.15), (2.16) and (4.31), respectively. Following a decomposition for the mean Hiemenz velocity ϕ

$$\phi(\eta) = \phi^{p} + \phi^{b} = (\eta - \delta_{d}) + \phi^{b}, \tag{A 2}$$

the operators $\mathscr{L}_{u}$ and $\mathscr{L}_{\omega}$ can also be decomposed into

$$\left.\begin{aligned} \mathscr{L}_{\omega}(\phi, \omega) &= \mathscr{L}^{p}_{\omega}(\phi^{p}, \omega) + \mathscr{L}^{b}_{\omega}(\phi^{p}, \phi^{b}, \omega), \\ \mathscr{L}_{u}(\phi, v, u) &= \mathscr{L}^{p}_{u}(\phi^{p}, v, u) + \mathscr{L}^{b}_{u}(\phi^{p}, \phi^{b}, v, u), \end{aligned}\right\} \tag{A 3}$$

where the superscript p denotes the operator in which ϕ has been replaced by its potential form ϕ^{p}, and b denotes the complementary operator resulting from this decomposition; the effect of the Hiemenz boundary layer is thus incorporated in the $\mathscr{L}^{b}$ operators. The disturbances ω, u and v can also be naturally decomposed as

$$\omega = \omega^{p} + \omega^{b}, \qquad u = u^{p} + u^{b}, \qquad v = v^{p} + v^{b}. \tag{A 4}$$

For the p quantities, the governing equations are

$$\mathscr{L}^{p}_{\omega}(\phi^{p}, \omega^{p}) = 0, \qquad \mathscr{L}^{p}_{u}(\phi^{p}, v^{p}, u^{p}) = 0, \qquad \mathscr{L}_{v}(u^{p}, \omega^{p}, v^{p}) = 0. \tag{A 5a–c}$$

The governing equations for the b quantities follow directly from the decompositions in (A 3) and (A 4). For velocities u^p and v^p, we enforce the same boundary conditions as those for the original u and v, i.e.

$$u^p = 0 \quad \text{at} \quad \eta = 0, \quad \eta \to \infty, \tag{A 6}$$

$$v^p = 0, \quad \frac{\mathrm{d}v^p}{\mathrm{d}\eta} = 0 \quad \text{at} \quad \eta = 0. \tag{A 7}$$

For the ω^p, (4.30) leads to the first boundary condition

$$\omega^p \to \omega_\infty \qquad \text{as} \quad \eta \to \infty. \tag{A 8}$$

where ω_∞ is the initial disturbance vorticity introduced far upstream. The second boundary condition for ω^p can be derived from the fact that as $\eta \to \infty$

$$v^p \to \begin{cases} 1 & \text{for fundamental mode,} \\ 0 & \text{else,} \end{cases} \tag{A 9}$$

which is implied by (2.21). To see this, solving (A 5c) subject to the boundary condition (A 7), we obtain

$$v^p = -\frac{\exp(nk_0\eta)}{2} \int_0^\eta (\mathrm{i}\omega^p + u^p) \exp(-nk_0\eta')\, \mathrm{d}\eta' + \frac{\exp(-nk_0\eta)}{2} \int_0^\eta (\mathrm{i}\omega^p - u^p) \exp(nk_0\eta')\, \mathrm{d}\eta'. \tag{A 10}$$

For (A 9) to be realizable, v^p must remain bounded as $\eta \to \infty$. So the coefficient of $\exp(nk_0\eta)$ in (A 10) must go to zero as $\eta \to \infty$, i.e.

$$\int_0^\infty (\mathrm{i}\omega^p + u^p) \exp(-nk_0\eta')\, \mathrm{d}\eta' = 0. \tag{A 11}$$

Moreover, notice that

$$u^p \equiv 0 \tag{A 12}$$

as a result of $(\phi^p)'' \equiv 0$ in $\mathscr{L}_u^p$ and the homogeneous boundary condition (A 6). Thus, (A 11) reduces to

$$\int_0^\infty \omega^p \exp(-nk_0\eta')\, \mathrm{d}\eta' = 0, \tag{A 13}$$

which serves as the second boundary condition for ω^p. Since the general expression for ω^p has been obtained in (4.20), (A 8) and (A 13) can thus be used to specify the two arbitrary constants therein.

Once ω^p and v^p are known, the corresponding b quantities can be readily solved. Notice that, by construction, u^b and v^b satisfy homogeneous boundary conditions, and the boundary condition for ω^b for $\eta \to \infty$ is also homogeneous.

Appendix B. Vorticity asymptotes

The general asymptotic expression for the confluent hypergeometric function with large real argument is (Abramowitz & Stegun 1970)

$$M(a; c; -z) = \frac{\Gamma(c)}{\Gamma(c-a)}\, z^{-a} \left[1 + O(|z|^{-1})\right] \quad \text{as} \quad z \to \infty;\, ph(z) = 0. \tag{B 1}$$

Since the inflow boundary is assumed to be far upstream, i.e. $H_0 \gg 1$, the asymptotic expressions for M_1 and M_2 in (4.34) are as follows.

$$M_1 \sim \frac{\Gamma\left(\frac{1}{2}\right)}{\Gamma\left(n^2/2\lambda + \frac{1}{2}\mathrm{i}m\sigma_0\right)}\left(\frac{H_0}{\sqrt{2}}\right)^{n^2/\lambda - 1 + \mathrm{i}m\sigma_0}, \tag{B 2a}$$

$$M_2 \sim \frac{\sqrt{2}\Gamma\left(\frac{3}{2}\right)}{\Gamma\left((\lambda + n^2)/2\lambda + \frac{1}{2}\mathrm{i}m\sigma_0\right)}\left(\frac{H_0}{\sqrt{2}}\right)^{n^2/\lambda - 1 + \mathrm{i}m\sigma_0}. \tag{B 2b}$$

When $\lambda \to \infty$, by the nature of the Γ function on a complex plane, $|\Gamma(z)|$ decrease rapidly along the imaginary axis. So (B 2) shows that for large λ, $M_2 \gg M_1$. Moreover, $|I_1|$ and $|I_2|$ in (4.36) can be shown to be of the same order of magnitude, thus compared to $|I_1|/|I_2|M_2$, M_1 can be neglected. Substituting these relations into (4.35) yields the asymptotic expression for the amplitudes of C_{mn} and D_{mn} at large λ:

$$C_{mn} \sim -\frac{\Gamma\left(\frac{1}{2} + n^2/2\sigma_0 + \frac{1}{2}\mathrm{i}m\sigma_0\right)}{\sqrt{2}\Gamma\left(\frac{3}{2}\right)}\frac{I_2}{I_1}\left(\frac{H_0}{\sqrt{2}}\right)^{1 - n^2/\lambda - \mathrm{i}m\sigma_0}, \tag{B 3a}$$

$$D_{mn} \sim \frac{\Gamma\left(\frac{1}{2} + n^2/2\lambda + \frac{1}{2}\mathrm{i}m\sigma_0\right)}{\sqrt{2}\Gamma\left(\frac{3}{2}\right)}\left(\frac{H_0}{\sqrt{2}}\right)^{1 - n^2/\lambda - \mathrm{i}m\sigma_0}. \tag{B 3b}$$

In order to evaluate ω_{mn} at the wall, the amplitudes of C_{mn} and D_{mn} may be estimated more explicitly if the fundamental frequency σ_0 is low. In fact, for the Γ function of a complex argument, it follows

$$|\Gamma(a + \mathrm{i}\,b)| = \prod_{k=0}^{\infty}\frac{|a + k|}{|a + k + \mathrm{i}\,b|}|\Gamma(a)|, \tag{B 4}$$

and as $\sigma_0 \ll 1$, it becomes

$$\Gamma\left(\frac{1}{2} + \frac{n^2}{2\lambda} + \mathrm{i}\frac{m\sigma_0}{2}\right) \sim \frac{\Gamma\left(\frac{1}{2} + n^2/2\lambda\right)}{\sqrt{1 + \alpha_n m^2\sigma_0^2/4}} \tag{B 5}$$

where

$$\alpha_n = \sum_{k=0}^{\infty}\frac{1}{\left(k + \frac{1}{2} + n^2/2\lambda\right)^2}.$$

Substitute these expressions into (B 3*a*), and expand the Γ function in terms of power series of n^2/λ and $m^2\sigma_0^2$ up to the first order, then we have

$$\begin{aligned}|C_{mn}| &\sim \frac{|I_2|\Gamma\left(\frac{1}{2} + n^2/2\lambda\right)}{|I_1|\sqrt{2}\Gamma\left(\frac{3}{2}\right)\sqrt{1 + \alpha m^2\sigma_0^2/4}}\left(\frac{H_0}{\sqrt{2}}\right)^{1 - n^2/\lambda} \\ &\sim \frac{|I_2|}{|I_1|}H_0^{1 - n^2/\lambda}\left[1 + a_1\frac{n^2}{\lambda}\right]\left[1 - \frac{\alpha_n m^2}{8}\sigma_0^2\right] \\ &\sim H_0\left[1 + (a_1 - \ln H_0)\frac{n^2}{\lambda}\right]\left[1 - \frac{\alpha_n m^2}{8}\sigma_0^2\right],\end{aligned} \tag{B 6}$$

where $a_1 = (\ln 2 + \gamma)/2$ and $\gamma = 0.5772156\cdots$ is the Euler constant. The expression for $|D_{mn}|$ can be similarly obtained. Notice that the value of $|I_1|/|I_2|$, as mentioned before, is slow-varying and of order one. For instance, in the limit of low frequency

and large scale, i.e. $\sigma_0 \to 0$ and $\lambda \to \infty$,

$$I_1 \sim \sqrt{\frac{\pi e}{2}}\left[1 - \mathrm{erf}\left(\frac{\sqrt{2}}{2}\right)\right]; \qquad I_2 \sim \frac{\sqrt{e}}{2}\mathrm{Ei}\left(1, \tfrac{1}{2}\right) \tag{B 7}$$

where erf and Ei are the error function and exponential integral, we have therefore $|I_2|/|I_1| \to 0.70378178\cdots$. To simplify the discussion, the dependence of I_1/I_2 on λ and σ_0 will be neglected, i.e. $|I_1|/|I_2|$ is treated as a constant.

REFERENCES

Abramowitz, M. & Stegun, I. A. (ed.) 1970 *Handbook of Mathematical Functions with Formulas, Graphs, and Mathematical Tables*. Dover.

Ames, F. E. 1997 The influence of large-scale high-intensity turbulence on vane heat transfer. *J. Turbomach.* **199**, 23–30.

Ames, F. E., Wang, C. & Barbot, P. A. 2002 Measurement and prediction of the influence of catalytic and dry low NOx combustor turbulence on vane surface heat transfer. In *Proc. ASME TURBO EXPO 2002, GT-2002-30524, Amsterdam.*

Andreotti, B., Douady, S. & Couder, Y. 2001 An experiment on two aspects of the interaction between strain and vorticity. *J. Fluid Mech.* **444**, 151–174.

Bae, S., Lele, S. K. & Sung, H. J. 2003 Direct numerical simulation of stagnation region flow and heat transfer with free-stream turbulence. *Phys. Fluids* **15**, 1462–1484.

Batchelor, G. K. 1967 *An Introduction to Fluid Dynamics*. Cambridge University Press.

Batchelor, G. K. & Proudman, I. 1954 The effects of rapid distortion of a fluid in turbulent motion. *Q. J. Mech. Appl. Maths* **7**, 83–103.

Böttcher, J. & Wedemeyer, E. 1989 The flow downstream of screens and its influence on the flow in the stagnation region of cylindrical bodies. *J. Fluid Mech.* **204**, 501–522.

Dhanak, M. R. & Stuart, J. T. 1995 Distortion of the stagnation-point flow due to cross-stream vorticity in the external flow. *Phil. Trans. R. Soc. Lond.* A **352**, 443–452.

Goldstein, R. J. (ed.) 2001 *Heat Transfer in Gas Turbine Systems*. New York Academy of Sciences.

Grosch, C. E. & Salwen, H. 1982 Oscillating stagnation point flow. *Proc. R. Soc. Lond. A* **384**, 175–190.

Hunt, J. C. R. 1973 A theory of turbulent flow round two-dimensional bluff bodies. *J. Fluid Mech.* **61**, 625–706.

Isaacson, E. & Keller, H. B. 1993 *Analysis of Numerical Methods*. Dover.

Kerr, O. S. & Dold, J. W. 1994 Periodic steady vortices in a stagnation-point flow. *J. Fluid Mech.* **276**, 307–325.

Kestin, J. 1966 The effect of free-stream turbulence on heat transfer rates. In *Advances in Heat Transfer* (ed. T. F. Irvine & J. P. Hartnett), vol. 3. Academic.

Kestin, J. & Wood, R. T. 1970 On the stability of two-dimensional stagnation flow. *J. Fluid Mech.* **44**, 461–479.

Lighthill, M. J. 1954 The response of laminar skin friction and heat transfer to fluctuations in the stream velocity. *Proc. R. Soc. Lond.* A **224**, 1–23.

Lin, R. S. & Malik, M. R. 1996 On the stability of attachment-line boundary layers. Part 1. The incompressible swept Hiemenz flow. *J. Fluid Mech.* **311**, 239–255.

Lyell, M. J. & Huerre, P. 1985 Linear and nonlinear stability of plane stagnation flow. *J. Fluid Mech.* **161**, 295–312.

Merchant, G. J. & Davis, S. H. 1989 Modulated stagnation-point flow and steady streaming. *J. Fluid Mech.* **198**, 543–555.

Morkovin, M. V. 1979 On the question of instabilities upstream of cylindrical bodies. *NASA Contractor Rep.* **3231**.

Nagib, H. M. & Hodson, P. R. 1978 Vortices induced in a stagnation region by wakes. In *Aerodynamic Heating and Thermal Protection Systems* (ed. L. S. Fletcher), *Progress in Astronautics and Aeronautics*, vol. 59. AIAA.

Nakayama, W. 1995 Heat transfer engineering in systems integration: outlook for closer coupling of thermal and electrical design of computers. *IEEE Trans. Components Packaging Manufact. Technol.* A **18**, 818–826.

Sadeh, W. J. & Brauer, H. J. 1980 A visual investigation of turbulence in stagantion flow about a circular cylinder. *J. Fluid Mech.* **99**, 53–64.

Smith, M. C. & Kuethe, A. M. 1966 Effects of turbulence on laminar skin friction and heat transfer. *Phys. Fluids* **9**, 2337–2344.

Spalart, P. R. 1989 Direct numerical study of leading-edge contamination. *AGARD Conf. Proc.* **438** (5.1–13).

Sutera, S. P. 1965 Vorticity amplification in staganation-point flow and its effect on heat transfer. *J. Fluid Mech.* **21**, 513–534.

Theofilis, V., Fedorov, A., Obrist, D. & Dallmann, U. C. 2003 The extended Görtler–Hämmerlin model for linear instability of three-dimensional incompressible swept attachment-line boundary-layer flow. *J. Fluid Mech.* **487**, 271–313.

Van Dyke, M. 1975 *Perturbation Methods in Fluid Mechanics*. Parabolic Press, Stanford, CA.

Van Fossen, G. J., Simoneau, R. J. & Ching, C. Y. 1995 Influence of turbulence parameters, Reynolds number and body shape on stagnation region heat transfer. *J. Heat Transfer* **117**, 593–603.

Wilson, S. D. R. & Gladwell, I. 1978 The stability of a two-dimensional stagnation flow to three-dimensional disturbances. *J. Fluid Mech.* **84**, 517–527.

Xiong, Z. 2004 Stagnation point flow and heat transfer under free-stream turbulence. PhD thesis, Stanford University.

Xiong, Z. & Lele, S. K. 2001 Numerical study of leading-edge heat transfer under free-stream turbulence. *AIAA Paper 2001-1016*.